# Epigenetic insights into GABAergic development in Dravet Syndrome iPSC and therapeutic implications

Jens Schuster[1,#], Xi Lu[1, #], Yonglong Dang[1,#], Joakim Klar[1], Amelie Wenz[1], Niklas Dahl[1,*], Xingqi Chen[1,*]

[1]Department of Immunology, Genetics and Pathology, Uppsala University and Science for Life Laboratory, Uppsala, Sweden

# Equal contribution

* Corresponding author: xingqi.chen@igp.uu.se or niklas.dahl@igp.uu.se

**Key words**

Dravet syndrome, epilepsy, Chromatin accessibility, iPSC modeling, neuronal differentiation, epigenetic profiling, valproic acid

**Abstract**

Dravet syndrome (DS) is a devastating early onset refractory epilepsy syndrome caused by variants in the *SCN1A* gene. A disturbed GABAergic interneuron function is implicated in the progression to DS but the underlying developmental and pathophysiological mechanisms remain elusive, in particularly at the chromatin level. In this study, we utilized induced pluripotent stem cells (iPSCs) derived from DS cases and healthy donors to model disease-associated epigenetic abnormalities of GABAergic development. Employing the ATAC-Seq technique, we assessed chromatin accessibility at multiple time points (Day 0, Day 19, Day 35, and Day 65) of GABAergic differentiation. Additionally, we elucidated the effects of the commonly used anti-seizure drug valproic acid (VPA) on chromatin accessibility in GABAergic cells. The distinct dynamics in chromatin profile of DS iPSC predicted accelerated early GABAergic development, evident at D19, and diverged further from the pattern in control iPSC with continued differentiation, indicating a disrupted GABAergic maturation. Exposure to VPA at D65 reshaped the chromatin landscape at a variable extent in different iPSC-lines and rescued the observed dysfunctional development in some DS iPSC-GABA. This study provides the first comprehensive investigation on the chromatin landscape of GABAergic differentiation in DS-patient iPSC, offering valuable insights into the epigenetic dysregulations

associated with interneuronal dysfunction in DS. Moreover, our detailed analysis of the chromatin changes induced by VPA in iPSC-GABA holds the potential to improve development of personalized and targeted anti-epileptic therapies.

## Introduction/Background

Dravet syndrome (DS) is an early onset and intractable epilepsy with an unfavorable long-term outcome. The first seizures are usually triggered by fever within the first 12 months of life[1,2]. Characteristic clinical features are age-related progression of seizures, cognitive decline, behavioral problems and movement disorder. The complex neurological symptoms associated with DS suggest underlying pathophysiological mechanisms that interfere with brain development[1-4]. Approximately 80% of DS cases carry heterozygous variants in the *SCN1A* gene encoding the α-subunit voltage-gated sodium channel (Nav1.1)[1,5]. Prior insights on the neuropathophysiology in DS have come from the *Scn1a* heterozygous mice, indicating a vital role of cortical interneurons in the pathogenesis. Mice with Nav1.1 haploinsufficiency in GABAergic interneurons exhibit spontaneous seizures and behavioral abnormalities[6-9] that are associated with subnormal sodium currents and impaired excitability of inhibitory interneurons[10,11]. Additionally, human iPSC derived neural cells carrying distinct pathogenic *SCN1A* variants have recapitulated electrophysiological and molecular perturbations in DS[12-16]. In combination, these studies have confirmed that *SCN1A* variants cause delayed sodium currents in activated and mainly inhibitory GABAergic interneurons, supporting the notion that seizures in DS are caused by deficient cortical inhibition[12].

Interneuronal progenitors emerge from the embryonic subpallium, mainly the median ganglionic eminence, and migrate tangentially to cortical progenitor zones. The second half of gestation is a period of rapid development of the human cortical GABAergic system that continues after term[17,18]. The extended developmental processes into mature GABAergic interneurons require continuous and complex remodeling of the chromatin structure for transcriptional adaptations[19]. While it is now clear that the distinct features in DS is associated with a reduced sodium current density in Nav1.1 haploinsufficient interneurons and a disinhibition of the cortical network[6,13,20], the underlying epigenetic mechanisms are poorly understood.

68 Treatment of DS patients is challenging and seizure control is rarely attainable[21]. The most
69 frequently used first-line drug is valproic acid (VPA)[1]. However, more than 50% of DS patients
70 are drug resistant without any decrease in seizure-frequency upon treatment[1], indicating
71 endogenous and subject-specific responses to VPA. The mechanisms by which VPA act are not
72 fully understood, but studies suggest that the drug inhibits histone deacetylase (HDAC) with an
73 impact on chromatin structure and gene expression[22,23]. Furthermore, a direct interaction of
74 VPA with sodium- or calcium-gated ion channels (e.g. Nav1.1) and enzymes crucial for GABA
75 turnover has been proposed[22]. While these studies have brought important information on the
76 mode of action of VPA[24-28], the specific effects of VPA on chromatin architecture of inhibitory
77 GABAergic interneurons have not yet been investigated to our knowledge.
78
79 We recently established induced pluripotent stem cell (iPSC) lines carrying distinct disease-
80 causing variants in the *SNC1A* gene and modeled GABAergic interneuron development in
81 DS[13,29]. The DS-patient iPSC derived GABAergic neurons recapitulated electrophysiological
82 abnormalities and gene expression analysis showed enrichment for histone modifications,
83 suggesting epigenetic abnormalities[13]. We therefore sought to explore the dynamics of open
84 chromatin in our DS-model of GABAergic development in DS using the assay of transposase
85 accessible chromatin sequencing (ATAC-Seq). The methodology has previously been used to
86 study chromatin accessibility of annotated genes during brain development[30-32] and, specifically,
87 in interneuronal differentiation[19,33]. Herein, we employed ATAC-Seq to investigate the
88 dynamics of chromatin accessibility in iPSC of DS-patients and healthy donors at four different
89 time points (Day 0, Day 19, Day 35, and Day 65) of GABAergic development. Moreover, we
90 explored the effect of VPA on chromatin accessibility in GABAergic neurons. Our study
91 uncovered accelerated chromatin changes in DS patient cells during the initial phase of
92 GABAergic development (up to Day 19) when compared to cells of healthy donors. Further
93 differentiation revealed that DS-patient GABAergic cells acquire a distinct chromatin profile
94 when compared to that of control cells. Notably, VPA treatment of GABAergic neurons leads
95 to unspecific genome-wide changes in chromatin architecture that predicts a promoted
96 GABAergic development in some iPSC lines. This study represents the first investigation of
97 the chromatin dynamics of GABAergic development in DS-patient iPSC, shedding light on the
98 underlying epigenetic abnormalities. Moreover, the in-depth characterization of chromatin
99 changes in GABAergic neurons induced by VPA may bring important information for the
100 development of individualized anti-seizure therapies.
101

102 **Results**

103 **Dynamic chromatin accessibility in an iPSC model of GABAergic development**

104 We previously established a protocol for GABAergic interneuronal differentiation of iPSC[13,29].
105 Analysis of RNAseq data at D19 and D65 of GABAergic differentiation revealed *SCN1A*
106 expression in neuronal cells derived from healthy donors and from patients with Dravet disease
107 (**Supplementary Figure 1A**). The *SCN1A* expression was confirmed with qPCR at D19, D35,
108 and D65 of differentiation whereas no expression could be detected in undifferentiated iPSC
109 (D0; **Supplementary Figure 1B**). We then applied ATAC-Seq to investigate the dynamics of
110 chromatin accessibility in GABAergic development associated with *SCN1A* variants. We first
111 obtained a reference for chromatin accessibility changes during GABAergic interneuronal
112 differentiation in iPSC from three healthy donors (Ctl) using ATAC-Seq[35] (**Figure 1A**). The
113 differentiating cultures were collected at four distinct time points of differentiation at day 0 (D0;
114 termed iPSC), D19 (neural progenitor cells; NPC), D35 (intermediate neuronal cells; imN) and
115 D65 (GABAergic interneurons; GABA). The cultures displayed expression of marker genes
116 confirming the development into GABAergic interneurons[13]. As previously shown, cultures
117 stained positive for pluripotent stem cell markers such as NANOG, SOX2, and OCT4 at D0.
118 The expression of these markers decreased upon neural induction and disappeared with further
119 differentiation. Markers for neural progenitor cells (FOXG1, PAX6) were expressed at D19
120 followed by the expression of immature neuronal cell markers (DCX and NKX2.1) at D35 and
121 of markers for GABAergic interneurons (GAD1, TUBB3) at D65 (**Supplementary Figure 1C**
122 **and Schuster et al. 2019[13]**).

123

124 The quality of ATAC-Seq data from each sample was validated by sequencing depth
125 comparison, genome-wide correlation between technical replicates and by calculating the
126 fraction of reads in enriched peaks (FRiP), the transcription start site enrichment score
127 (**Supplementary Figure 2A-D**). We captured accessible chromatin peaks at each time-point of
128 differentiation: 58,382 peaks at D0 (Ctl-iPSC), 68,002 peaks at D19 (Ctl-NPC), 52,933 peaks
129 at D35 (Ctl-iMN), and 74,561 peaks at D65 (Ctl-GABA) (**Supplementary Table 1**). Genomic
130 annotation of the accessible chromatin sites with respect to promoters, introns and exons
131 revealed a heterogenous distribution in iPSC, NPC, imN and GABA (**Supplementary Figure**
132 **2E).** Furthermore, principal component analysis (PCA) of chromatin accessibility at the four
133 time points demonstrated that the three biological replicates separated into four clusters
134 corresponding to each of the four time points of GABAergic development (**Supplementary**
135 **Figure 2F**), albeit with some degree of variability at the intermediate time points (D19 (NPC)

136 and D35 (imN)), possibly reflecting cell line specific and endogenous differences reported
137 previously[36]. We therefore treated the three Ctl-iPSC-lines as biological replicates for
138 downstream analysis. We also performed genome-wide correlation of ATAC-Seq with our
139 previously published RNA-Seq data at D19 and D65 (**Supplementary Figure 2G**). The
140 correlation ranged between 0.52 and 0.57, further indicating the good quality of the ATAC-Seq
141 data.
142 We then characterized changes in chromatin accessibility during GABAergic development in
143 Ctl-iPSC. The ATAC-Seq peaks in iPSC (D0) were used as reference and compared to the
144 accessible peaks in NPC, imN and GABA. To avoid capturing the dynamic changes of
145 accessible regions caused by variability across individuals, we initially compared the dynamic
146 changes of chromatin accessibility cell line by cell line across differentiation. Subsequently, we
147 extracted the common changes observed across different cell lines at each time point (**Methods**).
148 In total, we identified 19,931 significant differential peaks (|log2(fold change (FC))|> 1, false
149 discovery rate (FDR) < 0.01) (**Supplementary Figure 3A, Methods**). Next, we employed an
150 unbiased cluster method to investigate the dynamics of these differential accessible peaks,
151 resulting in the identification of four distinct clusters (Cluster 1-4) (**Figure 1B, Supplementary**
152 **Figure -3B-D**). Cluster 1 (n=9,565) consisted of peaks that were open D0 (cluster Ctl-iPSC)
153 and that gradually closed during differentiation. Cluster 2 (n=3,285) contained peaks that were
154 predominantly open at D19 (cluster Ctl-NPC). Cluster 3 (n=3,533) exhibited a high chromatin
155 accessibility at both D19 and D35 (cluster Ctl-imN) but more closed at D65. Cluster 4 (n=3,545)
156 displayed the highest accessibility specifically at D65 (cluster Ctl-GABA; **Figure 1B, 1C**). A
157 genomic annotation of the differential peaks in the four clusters with respect to promoters,
158 exons, introns and distal regulatory sequences revealed differences mainly in introns and
159 promoter regions. The Ctl-NPC cluster and Ctl-GABA cluster showed the highest proportion
160 of open chromatin in introns (45.6% and 43.4%, respectively) whereas in the Ctl-iPSC and Ctl-
161 imN clusters most accessible peaks were located in promoter regions (41.9% and 50.8%,
162 respectively; **Figure 1D**).
163
164 We then performed transcription factor (TF) enrichment analysis on the differential peaks
165 specific to each cluster (**Figure 1E**). The Ctl-iPSC cluster showed specific enrichment for
166 motifs of TFs for pluripotency, such as BRN1, OCT6, among others (**Figure 1E**), whereas
167 motifs for the SOX family of TFs were enriched in the Ctl-NPC-cluster. Ctl-NPC-specific
168 transcription factor motifs (e.g., SOX family TFs) were detected in the NPC-specific cluster.
169 Notably, motifs for common TFs (e.g., LHX family TFs, NKX6, RFX) as well as unique TFs

170 (e.g. SOX9, NF1 and DLX3) were enriched in both the Ctl-imN-specific cluster and the Ctl-
171 GABA specific cluster. The SOX family of TFs are important regulators of neuronal
172 development[37] and DLX factors function in orchestrating transcriptional activity during cortical
173 GABAergic development[38]. The temporal pattern of accessible and enriched TF motifs in our
174 differentiating Ctl-iPSC cultures is thus consistent with the TFs required for neuronal and
175 cortical GABAergic development *in vivo*, confirming our model system to be relevant.
176
177 Furthermore, we examined the biological processes associated with each cluster by assigning
178 each differential peak to the nearest gene. The annotated genes were then used for KEGG
179 analysis of each cluster (**Figure 1F, Supplementary Table 2**). In the Ctl-iPSC cluster we
180 identified enrichment of pathways related to pluripotency, such as signaling regulating
181 pluripotency of stem cells, while the Ctl-GABA cluster showed exclusive enrichment for
182 pathways for GABAergic neurons, such as GABAergic synapse and Neurotrophin signaling
183 (**Figure 1F**). Genome traces of annotated genes in each cluster validated the differential
184 accessible chromatin, e.g. for *NANOG* in the Ctl-iPSC cluster, *PAX6* and *GAD2* in the Ctl-NPC
185 and Ctl-imN clusters, respectively, and *GABRG3* in the Ctl-GABA cluster (**Figure 1G**). Gene
186 expression analysis of RNA-seq data at D19 and D65, as well as with qPCR at D0, D19, D35,
187 and D65, indicated that expression levels of the four genes was consistent with the chromatin
188 accessibility patterns (**Supplementary Figure 3E**). Taken together, these findings show that
189 the captured chromatin dynamics comply with the induction and development of GABAergic
190 neurons.
191
192 **Dynamic chromatin accessibility in a DS-iPSC model of GABAergic development**
193 Next, to gain a deeper understanding of chromatin dynamics during GABAergic development
194 associated with DS, we used the same strategy as above for differentiation and ATAC-Seq
195 analysis of iPSC-lines derived from the three DS patients (**Figure 2A, Supplementary Figure**
196 **4**). Unfortunately, one of the DS-iPSC lines (DD4A) did not differentiate up to D65 for
197 unknown reasons why data at this specific time-point are based on two DS-iPSC lines.
198 The ATAC-Seq data showed high quality and reproducibility at all four time-points
199 (**Supplementary Figure 4A-D**). In total, we detected 89,363 peaks in DS-iPSC, 79,270 peaks
200 in DS-NPC, 113,519 peaks in DS-imN, and 41,665 peaks in DS-GABA (**Supplementary**
201 **Table 3**). The genomic distribution of these accessible chromatin peaks with respect to
202 promoters, introns and exons showed deviations when compared to Ctl-iPSC lines, mainly at
203 D35 (DS-imN) and at D65 (DS-GABA) (**Supplementary Figure 4E**). Furthermore, the PCA

204 of chromatin accessibility in DS-iPSC replicates showed that they clustered together at D0, D19
205 and D35 (**Supplementary Figure 4F**). Notably, the clusters at D19 (iPSC-NPC) and at D35
206 (iPSC-imN) showed a strong overlap in contrast to the well distributed clusters at all four time
207 points in Ctl-iPSC lines (**Supplementary Figure 2F and 4F**). Genome-wide correlation of
208 ATAC-Seq and RNA-seq data at D19 and D65 showed good correlation (0.49 to 0.55;
209 **Supplementary Figure 4G**). The different dynamics of chromatin accessibility of DS-iPSC
210 lines when compared to that of Ctl-iPSC lines thus suggest a disrupted developmental trajectory
211 into DS-GABAergic interneurons consistent with an altered function of inhibitory GABAergic
212 interneurons in *Scn1a* heterozygous mice.
213
214 To further characterize chromatin changes in GABAergic differentiation of DS-iPSC lines, we
215 used the same strategy as for Ctl-iPSC lines by using the profile of chromatin accessibility in
216 DS-iPSCs (D0) as a reference. To avoid capturing the dynamic changes of accessible regions
217 caused by variability across individuals, we applied the same strategy as described for the
218 control samples (Methods). In total, we identified 19,896 differential peaks ($|\log2(FC)| > 1$,
219 FDR < 0.01) (**Methods**) that were clustered into four groups using an unbiased approach. The
220 four DS-specific clusters showed similar patterns as those of the Ctl group. The number of
221 accessible peaks were 8,517 at D0 (DS-iPSC), 4,317 at D19 (DS-NPC), 3,579 at D35 (DS-imN)
222 and 3,483 at D65 (DS-GABA) (**Figure 2B, 2C, Supplementary Figure 5A-D**). We identified
223 differences in the genomic distribution of the DS-iPSC clusters when compared to that in the
224 Ctl-iPSC clusters (**Figure 1D, 2D**). In the control group, 42.0% of the peaks were located in
225 promoter regions, whereas in the patient group, this proportion was slightly lower at 37.3%.
226 Additionally, a slightly higher proportion of DS-iPSC specific peaks were found in intron
227 regions (26.5%) compared to Ctl-iPSC (24.6%). The genomic features of the DS-NPC specific
228 cluster were similar between the Ctl group and the DS group. In the DS-imN specific cluster, a
229 lower proportion of peaks were located in promoter regions when compared to that of the Ctl
230 group (50.8% vs. 23.1%), while a lower proportion of peaks were from intron regions in the Ctl
231 group (27.8%) when compared to the DS group (46.2%). In the DS-GABA and Ctl-GABA
232 specific clusters, 34.7% and 25.9% of the peaks were located in promoter regions, respectively,
233 while 38.7% and 43.4% of the peaks were in intron regions in the Ctl and DS groups,
234 respectively.
235
236 We then examined the enrichment of motifs for trans-acting TFs within the differential peaks
237 of each DS-cluster at each time-point (**Figure 2E**). The DS-iPSC cluster specific peaks showed

238 enrichment of motifs from pluripotency related TFs, such as BRN1 and OCT4, whereas TF
239 motifs for the SOX family of TFs were enriched in both the DS-iPSC cluster and DS-NPC
240 cluster (**Figure 2E**). Peaks at TF motifs for LHX3 and NKX, specific for GABAergic neurons
241 were enriched only in the DS-NPC cluster but not in the DS-GABA cluster. However, the DS-
242 GABA specific peaks were enriched at motifs for the activator protein-1 (AP-1) family of TFs,
243 including JUN, FRA, and FOSL. Enriched motifs for the BACH2 TF were observed only in the
244 DS-GABA specific peaks and not in the Ctl-GABA peaks. Together, these data further support
245 that DS-iPSC, although they initially respond to our protocol for GABAergic induction with
246 accessible motifs for the SOX family of TFs, have a disrupted trajectory into GABAergic
247 interneurons as shown by the loss of motifs for DLX and LHX at D65.
248
249 Next, we annotated the differential accessible peaks to nearby genes and performed KEGG
250 pathway analysis for each cluster (**Figure 2F, Supplementary Table 4**). Similar to Ctl-iPSC,
251 the peaks of the DS-iPSC specific cluster were enriched for pathways related to pluripotency.
252 However, and in contrast to the control group, pathways related to GABAergic synapse were
253 enriched already in the DS-NPC specific clusters but not in the later appearing clusters specific
254 for DS-imN and DS-GABA (**Figure 2F**). Additionally, the pathway of long-term potentiation,
255 a hallmark for mature GABAergic cells, was specifically enriched in the DS-imN specific
256 cluster but not in the DS-GABA clusters. Furthermore, representative annotated genes for Ctl-
257 iPSC lines, PAX6 and GAD2 in the Ctl-NPC and Ctl-imN clusters, and GABRG3 in the Ctl-
258 GABA cluster, exhibit a different tendency of chromatin accessibility in DS-iPSC clusters
259 (**Figure 2G**), also shown by qPCR analysis (**Supplementary Figure 5E**). The enrichment of
260 TF motifs and predicted pathways relevant for GABAergic interneuron appearing already in
261 DS-NPC, but not in DS-GABA, uncovered a pattern distinct from that in Ctl-iPSC lines, that
262 strongly suggest a perturbed GABAergic development associated with *SCN1A* variants.
263
264 **Common chromatin dynamics in Ctl- and DS-iPSC models of GABAergic development**
265 Identification of abnormal chromatin dynamics in GABAergic interneuronal development of
266 DS-iPSC lines requires a thorough comparison with Ctl-iPSC lines. To extract shared dynamic
267 chromatin features in DS-patient and Ctl-iPSC lines we first merged the differentially accessible
268 chromatin peaks specific to each of the four time points (D0, D19, D35 and D65) within the Ctl
269 and DS patient groups, respectively. The lists of all significant peaks in the Ctl- and DS- iPSC
270 lines, respectively, were subsequently intersected to identify the common peak regions. In total,

271 we identified 12,256 accessible chromatin peaks that show a shared and time-point specific
272 pattern (**Figure 3A, Supplementary Table 5**).
273
274 Next, we sought to examine the genomic annotations, KEGG pathways, and TF motif
275 enrichment for these common peaks (**Figure 3**). A K-mean clustering of read counts from the
276 12,252 accessible chromatin peaks revealed four common clusters (Com-1 with 6,264 peaks,
277 Com-2 with 2,071 peaks, Com-3 with 1,793 peaks, and Com-4 with 2,124 peaks)
278 (**Supplementary Figure 6**, **Figure 3A**). The DS-iPSC and Ctl-iPSC lines show a similar
279 sequencing read count enrichment in Com-1 cluster and Com-2 clusters at the four time-points
280 whereas slight differences are observed for the Com-3 and Com-4 clusters (**Figure 3A**).
281 Accessible regions in Com-1 cluster are specifically open at D0 (iPSC) with annotations to TF
282 genes for pluripotency such as *NANOG* and *SOX2*, among others. The Com-1 cluster remains
283 closed at the following three time-points. The Com-2 cluster is closed at D0 but open at D19
284 (NPC) with accessible peaks at genes such as *MAP2*, *NEUROD1*, and *NEUROG1*, among
285 others (**Figure 3A**).
286
287 In both the Ctl and DS-patient groups, accessible regions in the Com-3 cluster are closed D0
288 but slightly open at D19 (NPC) and at D35 (imN) and then more closed at D65 (GABA).
289 However, the degree of openness for a large proportion of peaks is much higher in the DS-
290 patient group when compared to the Ctl group. Furthermore, at D65 (GABA) the Com-3 cluster
291 shows accessible regions at NPC-specific genes such as *MAP2* and *ATOH1* but not for
292 regulatory elements of GABAergic neuron-specific genes, such as *ASCL1*, *LHX6*, and *DLX2*,
293 among others. The absence of common open chromatin regions at regulatory elements for
294 GABAergic specific genes in the Ctl and DS-patient groups supports altered dynamics of
295 accessible chromatin at the late time-point GABAergic development in our model system.
296
297 The genomic distribution of accessible peaks with respect to promoters, exons and introns
298 varies between the Com-clusters (**Figure 3B**). The Com-1 cluster shows a relatively large
299 proportion of accessible chromatin regions from promoter regions (38.2%) when compared to
300 the other clusters (Com-2: 22.0%; Com-3: 20.8%, and Com-4: 30.5%). Conversely, the Com-1
301 cluster shows a relatively small proportion of accessible regions in intronic regions (25.8%)
302 when compared to Com-2, 3 and 4 clusters. However, the genomic distribution of accessible
303 peaks was very similar in the Com-2 and Com-3 clusters.
304

305 We then conducted KEGG analysis on genes within peaks of the four Com-clusters to
306 understand the common biological features of the Ctl- and DS-iPSC lines. We observed
307 enrichment for the pathways of transcriptional regulation of pluripotency, that included
308 *NANOG*, in Com-1 (**Figure 3C**) and of nitric oxide-stimulated guanylate cyclase that included
309 *MAP2* in Com-2 (**Figure 3D**). However, in the Com-3 or Com-4 clusters, characterized by an
310 increasing open chromatin with development, we did not find enrichment in pathways relevant
311 for GABAergic cells (**Figure 3D**). These observations further indicate similarities in the Ctl
312 and DS iPSC-lines in cellular processes up to D19 (NPC), but significant differences at D35
313 (imN) and D65 (GABA).
314
315 Furthermore, we examined the enrichment of motifs for trans-acting transcription factors (TFs)
316 from all common peaks and clustered TFs with a k-means method. The TF enrichment patterns
317 are similar in the Ctl and DS groups, and three TF clusters were observed. Cluster 1, containing
318 pluripotent-specific TFs such as OCT4 and KLF, among others, shows enrichment at iPSC in
319 both the control and DS patient groups (**Figure 3E, 3F**). Cluster 2, including TF motifs for the
320 NPC-specific TFs ESRRB and HNF4A, is enriched in iPSC (D19) and imN (D35) (**Figure 3E,**
321 **3F**), while some TFs relevant to GABAergic cells, such as NFAT and NF1, are enriched in D65.
322 No GABAergic neuron-specific TFs (e.g., DLX, LHX, ASCL) are observed. Taken together,
323 our data suggest similarities between Ctl- and DS-iPSC lines in accessible chromatin at loci for
324 TFs important for GABAergic induction and early development. However, the Ctl- and DS-
325 iPSC groups do not show similarities in the enrichment of TFs that are critical at later stages of
326 GABAergic maturation.
327
328 **Distinct chromatin features in DS-iPSC GABAergic development**
329 A PCA analysis of ATAC-Seq data at D0 demonstrated that profiles of chromatin accessibility
330 are similar in Ctl-iPSC and DS-iPSC-lines at d0 (iPSC) but different at d19 (NPC), d35 (imN),
331 and d65 (GABA) (**Figure 4A**). These data suggest a diverging and disrupted trajectory of
332 GABAergic development in our DS-iPSC model when compared to that in Ctl-iPSC.
333
334 To further understand the molecular regulators of dysfunctional GABAergic development in
335 DS-iPSC, we extracted the chromatin accessible peaks that were mutually exclusive in the Ctl-
336 and DS-iPSC lines at each time point (as described in the Methods section). The peaks were
337 categorized into a Ctl distinct peak list and a DS distinct peak list. In total, the Ctl distinct peak
338 list contained 3,311 accessible peaks (0 peaks at D0; 42 peaks at D19; 1,490 peaks at D35; and

339 1,779 peaks at D65), while the DS distinct peak list contained 4,434 accessible peaks (0 peaks
340 at D0; 13 peaks D19; 1,708 peaks D35; and 2,713 peaks D65) (**Figure 4B, Supplementary**
341 **Figure 7A**, **Supplementary Table 6**). These distinct peaks were located at different genomic
342 regions (**Figure 4C**). Furthermore, KEGG enrichment analysis of the distinct peaks at D65
343 revealed pathways specific to cortical neurons, such as GABAergic synapse, Glutamatergic
344 synapse, Dopaminergic synapse, and others, in Ctl-GABA but not in DS-GABA (**Figure 4D,**
345 **Supplementary Figure 7B**,).
346
347 Next, we combined the distinct peak lists of the Ctl- and DS-iPSC lines and calculated
348 enrichment of TF motifs using a systematic approach with chromVAR (chromatin variation
349 across regions)[39]. We then performed a non-hierarchical clustering of TFs enriched in the
350 distinct groups and identified three clusters (Dis-1, Dis-2, Dis-3) (**Figure 4E**). Cluster Dis-1
351 comprised two subclusters of TFs: Subcluster 1 included the OCT family of TFs (OCT2, OCT4,
352 OCT6) and BRN1, with enrichment restricted to D0 (iPSC) in the DS group whereas in the Ctl
353 group the enrichment was observed at D0, D35, and D65 but not at D19. Subcluster 2 included
354 the GABAergic specific TFs OLIGO2, ASCL1, NEUROD1, NEUROG2, NKX6.1, LHX2, and
355 others. These TFs were not enriched at any time-point in the DS group but enriched in the
356 control group at D35 and D65 (**Figure 4F**). In cluster Dis-2, TFs such as JUNB, AP-1, RUNX2,
357 and others were enriched in the DS group from d0 (iPSC) to D65 (GABA). However, in the Ctl
358 group enrichment for Dis-2 cluster was observed only at D0 (iPSC). Cluster Dis-3 is enriched
359 in both Ctl- and DS-iPSC for TFs of the TEAD family, AP-2 and NF-kappa beta. In the Ctl
360 group, this enrichment increased significantly in NPC and decreased (disappeared) in imN and
361 GABAergic neurons. Interestingly, the enrichment of these TFs in cluster Dis-1 persisted in the
362 DS group with development from NPC to GABA. The absent enrichment of GABA -specific
363 TF motifs at D65 in the DS group brings further support for a disrupted chromatin remodeling
364 during interneuron development.
365
366 **VPA induces changes in the chromatin landscape of iPSC derived GABAergic**
367 **interneurons**
368 Valproic acid (VPA) is a broad-spectrum anti-epileptic drug commonly used in the treatment
369 of DS[1]. However, the response to VPA treatment varies considerable among affected
370 individuals[40]. Prior reports suggest that the drug acts as a histone deacetylase (HDAC) inhibitor
371 and thereby impacts chromatin remodeling[22,23]. We therefore hypothesized that chromatin
372 changes induced by VPA in GABAergic cells may uncover processes contributing to

373 therapeutic effects of the drug. To this end, we cultured Ctl- and DS-iPSC-derived GABAergic
374 interneurons at D65 with and without VPA supplementation at therapeutic concentrations for
375 six days. We then performed ATAC-Seq on three sample pairs of Ctl-GABA and on two pairs
376 of DS-GABA (**Figure 5A, Supplementary Figure 8A-D, Supplementary Table 7)**.
377 Subsequent PCA analysis of the ATAC-Seq data showed that VPA exposure induced variable
378 changes in accessible chromatin that were seemingly iPSC-line specific (**Figure 5B, 5C,**
379 **Supplementary Figure 8E**). We then focused our analysis on the sample pairs showing the
380 most extensive VPA-induced changes in chromatin accessibility, including two Ctl-GABA
381 pairs (Ctl1B and Ctl7C) and one DS-GABA pair (DD5A; **Figure 5C**). Genomic annotation
382 revealed that chromatin changes induced by VPA were distributed in promoters, introns, and
383 distal regulatory elements and at a variable extent when comparing individual Ctl and DS pairs
384 (**Supplementary Figure 8F**). The regions showing VPA induced changes in accessible
385 chromatin were distributed in promoters, introns, and distal regulatory elements (**Figure 5D**).
386 The changes in chromatin accessibility after VPA treatment observed in both the Ctl- and DS-
387 GABA may reflect unspecific effects of the drug. To validate our hypothesis on chromatin
388 specific effects of VPA we performed enrichment analysis of differentially accessible peaks for
389 each iPSC-GABA pair. The results show enrichment in chromatin-relevant pathways in both
390 Ctl and DS pairs (**Figure 5E**). The analysis of open chromatin in response to VPA in Ctl- and
391 DS-GABA thus suggest drug-induced changes that are unspecific and genome-wide. This is in
392 line with the reported unpredictable effects of VPA on seizure frequencies in DS.
393
394 Since VPA treatment has an effect on seizure frequencies in a subgroup of affected individuals,
395 we investigated whether VPA could "restore" the chromatin accessibility profile of DS-GABA
396 into the chromatin profile of Ctl-GABA. The pathways relevant for GABAergic cells became
397 enriched in the chromatin regions that become accessible after VPA treatment in the DS-GABA
398 sample pair (**Figure 5E**). A specific analysis of TF motifs becoming accessible in VPA-treated
399 DS-GABA uncovered enriched motifs for TFs relevant for GABAergic development, such as
400 LHX3, SOX and the RFX families of TFs (**Figure 5F**). Conversely, Ctl-GABA pairs showed
401 an opposite enrichment pattern for these TF motifs upon VPA treatment. Furthermore, both Ctl-
402 and DS-GABA showed a VPA-induced increase in chromatin accessibility at regulatory regions
403 of GABAergic specific genes, such as GAD1 and GABRG3 (**Figure 5G**). Taken together, our
404 iPSC model suggests that VPA has the potential to dramatically interfere with and change
405 chromatin structure in GABAergic cells. These changes are likely unspecific and may affect
406 genes important for interneuronal development.

407

408 **Discussion**

409 The majority of cases with DS are pharmaco-resistant and there is an urgent need to improve
410 our understanding of the underlying mechanisms for the development of targeted anti-seizure
411 treatments [2,40,41]. To this end, we used our iPSC-based model of GABAergic development in
412 DS caused by heterozygous *SCN1A* variants. The model system recapitulates hallmarks of the
413 disease and we therefore reasoned that it may improve our knowledge on DS-associated
414 epigenetic changes as well as chromatin modifications induced by the commonly used anti-
415 seizure drug VPA[13,29]. Specifically, we differentiated iPSCs from healthy donors (Ctl) and DS-
416 cases towards GABAergic cortical interneurons and characterized the dynamic chromatin
417 conformational changes using ATAC-Seq. To our knowledge, this is the first study that
418 describes chromatin accessibility changes in DS-patient derived iPSC neurodifferentiation. We
419 identified common and distinct chromatin accessibility profiles when comparing iPSC of DS
420 patients and healthy donors at different time points of GABAergic development. As expected,
421 the chromatin profiles of undifferentiated iPSC are similar in the two groups, with accessible
422 peaks for TF genes maintaining a pluripotent state, such as *NANOG* and *POU5F1*.
423 Differentiation towards a GABAergic fate shows that both Ctl and DS iPSC-lines acquire
424 accessible chromatin peaks associated with genes enriched in pathways relevant for
425 interneuronal development (e.g. signaling pathways, GABAergic synapse and long-term
426 potentiation). However, our analyses uncovered increased changes in accessible peaks at the
427 early phase (D19) of GABAergic development in DS-patient cells when compared to the
428 control group. At the same time-point (D19) we also detected expression of *SCN1A*, providing
429 a link between altered sodium flux and aberrant chromatin dynamics in DS-iPSC derived
430 neurons. The genes associated with the distinct temporal changes of open chromatin in DS-
431 patient cells are enriched in KEGG terms such as GABAergic synapse, Glutamatergic synapse
432 and Long-term potentiation, suggesting a perturbed and seemingly accelerated initial
433 GABAergic induction before D35. The enrichment in these pathways is lost with further
434 differentiation of DS derived iPSC-lines and they fail to acquire the chromatin profile of Ctl
435 GABAergic cells at D65. The aberrant chromatin profiles in our iPSC model comply with
436 previous studies on iPSC and mice models of DS showing both transcriptional and
437 electrophysiological changes in interneurons[9,13,42]. In our prior study, the transcriptional
438 changes emerged predominantly after D19, the ATAC-Seq analysis in the current study show
439 alterations in chromatin structure already at D19. This observation confirms that epigenetic
440 changes detected by ATAC-Seq precede the transcriptional changes[30]. Furthermore, our study

441 defines differential accessible chromatin regions and TF motifs associated with heterozygous
442 and pathogenic *SCN1A* variants, bringing further insights into disturbed interneuronal
443 differentiation in DS. In control iPSC lines, the chromatin accessibility of motifs for TFs
444 relevant to drive neurogenesis, such as NEUROG2, OLIG2, BRN1, increase with
445 differentiation whereas the same regions are closing in DS derived iPSC. On the other hand,
446 motifs of more general TFs, such as TEAD4, FOXM1, AP-2GAMMA, become either
447 accessible or un-accessible with differentiation in control iPSC but remain closed or open in
448 differentiating DS iPSC. This is consistent with our previous observations in DS-GABA
449 showing dysregulated expression of *FOXM1* and of genes enriched in pathways for histone
450 modification and cell cycle pathways[13]. Moreover, similar to the *Scn1a* +/- mice model,
451 showing an intact density of cortical and hippocampal GABAergic interneurons despite
452 impaired functions[20], our immunostainings revealed a comparable number and morphology of
453 DS-patient and Ctl GABAergic neurons. These observations suggest that the proliferative
454 capacity is relatively preserved during GABAergic interneuron development in DS.
455
456 Currently, valproic acid (VPA) is commonly used as one of the first line drugs in DS[1] but the
457 response on seizure frequencies is highly variable among affected cases[43,44]. The mode of action
458 of VPA is not fully understood but it is believed to inhibit histone deacetylases, leading to
459 changes in chromatin states and gene expression[25,45]. In our study, we aimed to study the
460 epigenetic effect of VPA administration on iPSC derived GABAergic neurons derived from DS
461 patients and healthy donors. The GABAergic interneurons exposed to therapeutic
462 concentrations of VPA for six days showed extensive changes in accessible chromatin peaks in
463 our cultures. Projection of the chromatin changes using KEGG uncovered pathways that reflect
464 the expected mode of action of VPA, such as *histone acetylation* and *deacetylation* and *rRNA*
465 *acetylation*, of importance for transcriptional activity.
466
467 However, the VPA-induced chromatin modifications in iPSC-GABA varied considerably with
468 biological origin and the accessibility changes linked to GABAergic development were
469 specific or shared for individual iPSC-GABA-lines. For example, in Ctl-GABA we observe an
470 enrichment for LHX1-3 and DLX3 motifs that changes from open to closed after VPA exposure.
471 In contrast, DS-GABA show a somewhat opposite enrichment pattern for LHX and DLX
472 binding motifs after VPA exposure that changes from closed to open. In mice, motifs for the
473 LHX and DLX family of TFs are enriched in the late interneuronal development that extends
474 postnatally[19]. In addition, Ctl-GABA show a reduction in accessible SOX-binding motifs after

475 VPA treatment whereas DS-GABA show an opposite response, acquiring a profile more similar
476 to the untreated Ctl-GABA. The SOX-family of TFs has a global impact on both embryonic
477 and adult neurogenesis[46] and enrichment of SOX binding motifs are enriched in migratory
478 interneurons[19]. These observations may suggest a mechanism by which VPA, at least in some
479 cases, facilitates accessibility for TFs with beneficial effects on postnatal GABAergic function.
480 Moreover, VPA treated DS-GABA uncovered enriched changes for TF motifs for AP-1 and
481 BRN1 that made the cells acquire a pattern more similar to that in control lines. It may therefore
482 be hypothesized that VPA induces unspecific changes in chromatin structure of iPSC-GABA
483 that, at least in some cases, may lead to an increased accessibility for TFs linked to GABAergic
484 development. Such a variability in response to VPA exposure in our model is consistent with
485 the unpredictable effects of VPA on seizure-frequencies, even in cases with identical *SCN1A*
486 variants[40], mediated by epigenetic factors that are specific to individuals. Finally, our iPSC
487 model of GABAergic development has limitations that should be considered. The model system
488 applies a directed protocol during 65d that may not fully recapitulate maturation of GABAergic
489 cells *in vivo*. Functional maturation of GABAergic interneurons occurs postnatally in humans,
490 and models using direct differentiation from iPSC typically do not reach into cellular states
491 comparable to postnatal cell types. More complex neuronal systems, such as 3D organoids from
492 isogenic iPSC lines and in long-term cultures, in combination with single cell analysis, will be
493 needed to confirm our data. Nevertheless, our findings represent an important step forward to
494 clarify epigenetic changes in inhibitory interneurons that are associated with the progression to
495 DS, adding data to a frame-work of knowledge for the development of targeted and
496 personalized therapies. Further studies are now required to increase the number of independent
497 iPSC lines with pathogenic *SCN1A* variants to validate our findings on epigenetic changes in
498 DS and the effects of anti-seizure drugs such as VPA.
499

500 **Materials and Methods**

501 **Cell culture, GABAergic differentiation and sampling**

502 iPSC lines from three patients (DD1C, DD4A, DD5A)[29] and three controls (Ctl1B, Ctl7C,
503 Ctl8F)[47] were cultured on human recombinant laminin LN521 (Biolamina) in Essential-8™
504 medium (Thermo Fisher Scientific) and passaged using Trypl Express (Thermo Fisher
505 Scientific) as described[29]. GABAergic interneuron differentiation from iPSCs was performed
506 as previously described[13]. The protocol utilizes DUAL SMAD inhibition to induce
507 neurogenesis towards neural stem cells for 10 days, followed by patterning with high levels of
508 sonic hedgehog for nine days towards cortically fated neuronal progenitor cells (NPC) that

509 mature for 46 days, i.e. a total of 65 days (Figure 1A). Neuronal cells at day 65 and onwards
510 are viable as judged by morphological assessment by light microscopy. Differentiation was
511 repeated at least three times per cell line.
512 Cell cultures were sampled at days 0 (D0), D19, D35 and D65, respectively, by harvesting cells
513 with TryplE and collecting by centrifugation (300 x g, 3 min). Harvested cells were counted
514 and assessed for viability using trypan blue staining and an automated EVE cell counter
515 (NanoEntek). Samples with a viability of >90% were selected for ATAC-Seq library
516 preparation (see below). Additionally, neuronal cell cultures at D65 were treated with valproic
517 acid (VPA; 0,5 mM) for 6 days and subsequently harvested for analysis. Harvested cells were
518 resuspended in 1 ml of 1 x PBS and fixed by adding an equal amount of 2% formaldehyde for
519 10 min at room temperature. The reaction was quenched by adding 100 ul 2,5 M glycine
520 solution. Fixed cells were collected by centrifugation and washed twice with 1 x PBS. Cells
521 where then resuspended in 1 x PBS, counted using an EVE automatic cell counter (NanoEntek)
522 with Trypan Blue, and subsequently 50'000 cells/sample were processed for library preparation
523 for ATAC sequencing.
524
525 **Tn5 transposome assembly**
526 Tn5 transposome assembly was performed by as previously described[48]. Briefly, 2 µM annealed
527 Tn5MErev/Tn5ME-A, 2 µM annealed Tn5MErev/Tn5ME-B, and 2 µM Tn5 transposase
528 (Protein Science Facility at Karolinska Institutet, Stockholm) in dialysis buffer (50 mM
529 HEPES-KOH at pH 7.2, 50 mM NaCl, 0.05 mM EDTA, 0,5 mM DTT, 0.05% Triton X-100, 5%
530 glycerol) with 40% glycerol were mixed, incubated for 1 h at room temperature and
531 subsequently stored at −20°C until use. The adaptor oligonucleotides (Tn5MErev: 5'-
532 /Phos/CTGTCTCTTATACACATCT-3', Tn5ME-A: 5′ -
533 TCGTCGGCAGCGTCAGATGTGTATAAGAGACAG-3′ and Tn5ME-B: 5′-
534 GTCTCGTGGGCTCGGAGATGTGTATAAGAGACAG-3′) were synthesized by Integrated
535 DNA Technology. For oligo annealing, equimolar amounts of Tn5MErev and Tn5ME-A or
536 Tn5ME-B and Tn5MErev, respectively, were combined in a PCR tube and annealed using the
537 following program: 95°C for 5 min, ramp down to 25°C with −0.1°C/s increments.
538
539 **ATAC-Seq library preparation and sequencing**
540 ATAC-Seq libraries were prepared following[48]. In brief, two technical replicates per sample
541 containing 50,000 nuclei each were collected at 500 x g for 5 min at 4°C. Nuclei were
542 resuspended in lysis buffer (10 mM Tris-Cl, pH 7.4; 10 mM NaCl; 3 mM MgCl2; 0.1% Igepal

543 CA-630) and centrifuged at 500 x g for 10 min. The supernatant was removed and each nuclei
544 pellet was resuspended in tagmentation buffer (25 µL 2 × TD buffer) with 2.5 µl Tn5
545 transposome and incubated at 37°C for 30 min. An equal volume of 2 x reverse crosslinking
546 buffer (50 mM Tris-Cl, 1mM EDTA, 1% SDS, 0.2M NaCl, 5 ng/ml Proteinase K) was added
547 to each sample and incubated at 65°C with agitation at 1200 rpm for overnight. DNA was
548 isolated using a MinElute PCR Purification Kit (Qiagen). Sequencing libraries were prepared
549 following described standard protocol[49]. All libraries were sequenced on an Illumina Nova-seq
550 platform at Novogene Europe.

551 **RNA isolation and quantitative RT-PCR**

552 Total RNA from iPSCs and differentiated cell populations was isolated using a miRNeasy
553 micro kit (Qiagen). 1 µg of total RNA was reverse transcribed into cDNA using High Capacity
554 cDNA transcription kit (ThermoFisher Scientific). Expression of marker genes was compared
555 to expression of the two housekeeping genes GAPDH and ACTB. FastStart Universal SYBR
556 Green Master mix (Roche) was used for qPCR using the following primers: ACTB-For:
557 CAGGAGGAGCAATGATCTTGATCT; ACTB-Rev, TCATGAAGTGTGACGTGGACATC;
558 GAPDH-For, GAAGGTGAAGGTCGGAGTC; GAPDH-Rev,
559 GAAGATGGTGATGGGATTTC; SCN1A-For, TGAAGAATCCAGGCAGAAATGC;
560 SCN1A-Rev, TCGAAATGAACGGAGAACAGA; NANOG-For,
561 CAGCCCCGATTCTCCACCAGTCCC; NANOG-Rev,
562 CGGAAGATTCCCAGTCGGGTTCACC; PAX6-For,
563 AACAGACACAGCCCTCACAAACA; PAX6-Rev, CGGGAACTTGAACTGGAACTGAC;
564 GAD2-For, AGCTGCAGCCTTAGGGATTG; GAD2-Rev, TTGCAAATGTCAGCGACAGC;
565 GABRG3-For, TCATGGGCCTCAGAAACACC; GABRG3-Rev,
566 CTTGCTGGCGTAGCATCTTTT. For all analyses, we used samples from three independent
567 differentiation cultures and each sample was analyzed in triplicate. Expression was calculated
568 as ΔCT(gene X, day Y) = CT(gene X, day Y) - CT(AVERAGE (GAPDH/ACTB, day Y)) and
569 fold change was calculated as ΔΔCT(gene X, day Y) = ΔCT(gene X, day Y) - ΔCT(gene X,
570 day 0) and presented as log2 [2ˆ-(ΔΔCT)] ±SD.

571

572 **Immunofluorescence staining**

573 Staining was performed on cells fixed with ice-cold 4% PFA and subsequently permeabilized
574 in blocking solution (1 x PBS pH 7.4, 1% BSA, 0.1% Triton X-100). Primary antibodies against
575 MAP2 (1:5’000; abcam, Cambridge, United Kingdom), GABA (1:1’000; Sigma, MO, United
576 States), GAD1 (1:100, Millipore, MA, United States) and DCX (1:100, Santa Cruz, United

577 States) were used for immunostaining and quantification. Primary antibodies were allowed to
578 bind overnight separately or in appropriate combinations at 4°C. After washing three times in
579 1 x PBS, the secondary antibodies donkey anti-goat IgG AlexaFluor 633, donkey anti-rabbit
580 IgG AlexaFluor 568 or donkey anti-mouse IgG AlexaFluor 488 (1:1'000; ThermoFisher
581 Scientific, Waltham, MA, United States) were applied alone or in appropriate combinations for
582 1.5 h at room temperature in the dark. Visualization was performed on a Zeiss 510 confocal
583 microscope (Carl Zeiss Microscopy, Jena, Germany) using Zen 2009 imaging software. Image
584 processing was carried out using FIJI software.
585
586 **Bioinformatic and statistical analyses**
587 **ATAC-Seq data processing and quality analysis**
588 After the Adapter sequence trimming, the ATAC-Seq sequencing reads were mapped to
589 genome hg38 using bowtie2[50]. Mapped paired reads were corrected for the Tn5 cleavage
590 position by shifting +4/-5 bp depending on the read strand. All mapped reads were extended to
591 50 bp centered around the Tn5 offset. PCR duplicates were removed using Picard
592 (http://broadinstitute.github.io/picard/), and sequencing reads from chromosome M were
593 filtered out. The Peak calling of each ATAC-Seq library was performed with MACS2[51] with
594 parameters -f BED, -g hs, -q 0.01, --nomodel, --shift 0. Peaks were merged into a matrix using
595 bedtools merge [52]. Raw reads within peaks were normalized using EdgeR's cpm function [53].
596 Log transformation was applied to these normalized peaks to calculate the Pearson correlation
597 among duplicates. Differential ATAC peaks for clusters were selected using DESeq2[54] with the
598 following cutoffs: false discovery rate (FDR) < 0.05, |log2 fold change| > 1, and peak average
599 intensity > 16. FDR values are Benjamini-Hochberg procedure corrected per default settings.
600
601 **Chromatin accessibility dynamic across differentiation**
602 To avoid capturing the dynamic changes of accessible regions caused by variability across
603 individuals, we initially compared the dynamic changes of chromatin accessibility cell line by
604 cell line across differentiation. Subsequently, we extracted the common changes observed
605 across different cell lines at each time point. Cluster analysis was conducted on both control
606 and patient groups of ATAC-Seq data at different time points during differentiation (D0, D19,
607 D35, and D65). The raw data were processed with background correction and normalization
608 using Reads Per Kilobase per Million mapped reads (RPKM). Clustering analysis was
609 performed separately for the control and patient groups of ATAC-Seq data using the Mfuzz
610 package[55], with minimum standard deviation and Z score parameters set at 1 and 0.5,

respectively. Clusters were assigned based on the chromatin accessibility patterns of differential chromatin accessible peaks. Subsequently, clusters exhibiting significant changes were selected for further analysis.

**Annotation of unique ATAC peaks to genes and KEGG pathway analysis**

Genomic annotation of each ATAC-Seq peak to its nearest gene for the differential accessible regions was done using ChIPseeker[56]. A gene promoter region was defined as 3 kb upstream and 3 kb downstream of the transcription start site. The peaks were annotated to their nearest gene within a 10 kb distance from the transcription start site (TSS). Subsequently, Clusterprofiler[57] was used to perform Kyoto Encyclopedia of Genes and Genomes (KEGG) pathway enrichment analysis, and the results were ranked by false discovery rate (FDR). An FDR of less than 0.05 was set as significant.

**Transcription factors (TFs) motif enrichment analysis**

TF motif enrichment was performed with HOMER [58] using the differential accessible regions as input. For TF binding prediction, chromVAR [39] was employed. In brief, the Homer vertebrate TF database was used as input for TF motifs in chromVAR, and then TF accessibility deviation values were calculated for each sample across the entire sample set. TF deviations with a threshold greater than 2 were retained, and TF motifs with a positive correlation with one group/cluster were selected to represent that group/cluster. TFs were ranked based on their variability within each group/cluster, and z-scores of deviations from each TF were visualized in a heatmap.

**Author contributions**

Conceptualization: JS, ND, XC; Methodology: JS, XL, YD, JK, AW; Analysis and Investigation: JS, XL, YD, JK, ND, XC; Data curation and Visualization: JS, XL, YD, JK; Writing – original draft: JS, XC; Writing – Review and Editing: JS, XL, JK, YD, ND, XC; Supervision: ND, XC; Funding Acquisition: ND, XC.

**Declaration of interest**

The authors declare that no conflicting interest exists.

**Acknowledgements**

Research in the lab is funded by the Swedish Research Council (2020-01947 to N.D. and 2022-00658 to X.C.), Hjärnfonden (FO2020-0171 and FO2022-0042 to ND), Swedish Cancer Foundation (21 1449Pj, 22 0491 JIA to X.C.), Stiftelsen Margarethahemmet (to N.D.) and Sävstaholm Society (to J.S.), Wallenberg Academy Fellow from Knut and Alice Wallenberg foundation (2023.0046 to X.C.), Uppsala University and Science for Life Laboratory. The funders played no role in study design, data acquisition and interpretation or decision to publish.

**Availability of the data**

The ATAC-Seq data generated for this study have been deposited in the Sequence Read Archive (SRA) with the following number: PRJNA1013337.

**References**

1 He, Z., Li, Y., Zhao, X. & Li, B. Dravet syndrome: Advances in etiology, clinical presentation, and treatment. *Epilepsy Res* **188**, 107041, doi:10.1016/j.eplepsyres.2022.107041 (2022).

2 Dravet, C. The core Dravet syndrome phenotype. *Epilepsia* **52 Suppl 2**, 3-9, doi:10.1111/j.1528-1167.2011.02994.x (2011).

3 Li, W., Schneider, A. L. & Scheffer, I. E. Defining Dravet syndrome: An essential pre-requisite for precision medicine trials. *Epilepsia* **62**, 2205-2217, doi:10.1111/epi.17015 (2021).

4 Ragona, F. Cognitive development in children with Dravet syndrome. *Epilepsia* **52 Suppl 2**, 39-43, doi:10.1111/j.1528-1167.2011.03000.x (2011).

5 Brunklaus, A. & Zuberi, S. M. Dravet syndrome--from epileptic encephalopathy to channelopathy. *Epilepsia* **55**, 979-984, doi:10.1111/epi.12652 (2014).

6 Cheah, C. S. *et al.* Specific deletion of NaV1.1 sodium channels in inhibitory interneurons causes seizures and premature death in a mouse model of Dravet syndrome. *Proc Natl Acad Sci U S A* **109**, 14646-14651, doi:10.1073/pnas.1211591109 (2012).

7 Kalume, F. *et al.* Sleep impairment and reduced interneuron excitability in a mouse model of Dravet Syndrome. *Neurobiol Dis* **77**, 141-154, doi:10.1016/j.nbd.2015.02.016

S0969-9961(15)00043-1 [pii] (2015).

676 8 Ito, S. *et al.* Mouse with Nav1.1 haploinsufficiency, a model for Dravet syndrome,
677 exhibits lowered sociability and learning impairment. *Neurobiol Dis* **49**, 29-40,
678 doi:10.1016/j.nbd.2012.08.003 (2013).
679 9 Han, S. *et al.* Autistic-like behaviour in Scn1a+/- mice and rescue by enhanced
680 GABA-mediated neurotransmission. *Nature* **489**, 385-390, doi:10.1038/nature11356
681 (2012).
682 10 Yu, F. H. *et al.* Reduced sodium current in GABAergic interneurons in a mouse model
683 of severe myoclonic epilepsy in infancy. *Nat Neurosci* **9**, 1142-1149, doi:nn1754 [pii]
684 10.1038/nn1754 (2006).
685 11 Tai, C., Abe, Y., Westenbroek, R. E., Scheuer, T. & Catterall, W. A. Impaired
686 excitability of somatostatin- and parvalbumin-expressing cortical interneurons in a
687 mouse model of Dravet syndrome. *Proc Natl Acad Sci U S A* **111**, E3139-3148,
688 doi:10.1073/pnas.1411131111 (2014).
689 12 Sun, Y. *et al.* A deleterious Nav1.1 mutation selectively impairs telencephalic
690 inhibitory neurons derived from Dravet Syndrome patients. *Elife* **5**,
691 doi:10.7554/eLife.13073
692 e13073 [pii] (2016).
693 13 Schuster, J. *et al.* Transcriptomes of Dravet syndrome iPSC derived GABAergic cells
694 reveal dysregulated pathways for chromatin remodeling and neurodevelopment.
695 *Neurobiol Dis* **132**, 104583, doi:10.1016/j.nbd.2019.104583 (2019).
696 14 Maeda, H. *et al.* Establishment of isogenic iPSCs from an individual with SCN1A
697 mutation mosaicism as a model for investigating neurocognitive impairment in Dravet
698 syndrome. *J Hum Genet* **61**, 565-569, doi:10.1038/jhg.2016.5
699 jhg20165 [pii] (2016).
700 15 Jiao, J. *et al.* Modeling Dravet syndrome using induced pluripotent stem cells (iPSCs)
701 and directly converted neurons. *Hum Mol Genet* **22**, 4241-4252,
702 doi:10.1093/hmg/ddt275
703 ddt275 [pii] (2013).
704 16 Higurashi, N. *et al.* A human Dravet syndrome model from patient induced pluripotent
705 stem cells. *Mol Brain* **6**, 19, doi:10.1186/1756-6606-6-19
706 1756-6606-6-19 [pii] (2013).

17 Arshad, A. *et al.* Extended Production of Cortical Interneurons into the Third Trimester of Human Gestation. *Cereb Cortex* **26**, 2242-2256, doi:10.1093/cercor/bhv074 (2016).

18 Xu, G. *et al.* Late Development of the GABAergic System in the Human Cerebral Cortex and White Matter. *J Neuropath Exp Neur* **70**, 841-858, doi:10.1097/NEN.0b013e31822f471c (2011).

19 Allaway, K. C. *et al.* Genetic and epigenetic coordination of cortical interneuron development. *Nature* **597**, 693-697, doi:10.1038/s41586-021-03933-1 (2021).

20 Ogiwara, I. *et al.* Nav1.1 haploinsufficiency in excitatory neurons ameliorates seizure-associated sudden death in a mouse model of Dravet syndrome. *Hum Mol Genet* **22**, 4784-4804, doi:10.1093/hmg/ddt331 (2013).

21 Aras, L. M., Isla, J. & Mingorance-Le Meur, A. The European patient with Dravet syndrome: results from a parent-reported survey on antiepileptic drug use in the European population with Dravet syndrome. *Epilepsy Behav* **44**, 104-109, doi:10.1016/j.yebeh.2014.12.028 (2015).

22 Ghodke-Puranik, Y. *et al.* Valproic acid pathway: pharmacokinetics and pharmacodynamics. *Pharmacogenet Genomics* **23**, 236-241, doi:10.1097/FPC.0b013e32835ea0b2 (2013).

23 Ximenes, J. C. M., Verde, E. C. L., Naffah-Mazzacoratti, M. G. & Viana, G. S. d. B. Valproic Acid, a Drug with Multiple Molecular Targets Related to Its Potential Neuroprotective Action. *Neuroscience and Medicine* **3**, 107-123, doi:10.4236/nm.2012.31016. (2012).

24 Balasubramanian, D., Pearson, J. F. & Kennedy, M. A. Gene expression effects of lithium and valproic acid in a serotonergic cell line. *Physiol Genomics* **51**, 43-50, doi:10.1152/physiolgenomics.00069.2018 (2019).

25 Jiang, X. *et al.* Sodium valproate rescues expression of TRANK1 in iPSC-derived neural cells that carry a genetic variant associated with serious mental illness. *Mol Psychiatry* **24**, 613-624, doi:10.1038/s41380-018-0207-1 (2019).

26 Wang, Y. & Li, Z. RNA-seq analysis of blood of valproic acid-responsive and non-responsive pediatric patients with epilepsy. *Exp Ther Med* **18**, 373-383, doi:10.3892/etm.2019.7538 (2019).

27 Golla, U., Joseph, D. & Tomar, R. S. Combined Transcriptomics and Chemical-Genetics Reveal Molecular Mode of Action of Valproic acid, an Anticancer Molecule using Budding Yeast Model. *Sci Rep* **6**, 35322, doi:10.1038/srep35322 (2016).

741 28 Balasubramanian, D., Deng, A. X., Doudney, K., Hampton, M. B. & Kennedy, M. A.
742 Valproic acid exposure leads to upregulation and increased promoter histone
743 acetylation of sepiapterin reductase in a serotonergic cell line. *Neuropharmacology* **99**,
744 79-88, doi:10.1016/j.neuropharm.2015.06.018 (2015).
745 29 Schuster, J. *et al.* Generation of three human induced pluripotent stem cell (iPSC)
746 lines from three patients with Dravet syndrome carrying distinct SCN1A gene
747 mutations. *Stem Cell Res* **39**, 101523, doi:10.1016/j.scr.2019.101523 (2019).
748 30 Inoue, F., Kreimer, A., Ashuach, T., Ahituv, N. & Yosef, N. Identification and
749 Massively Parallel Characterization of Regulatory Elements Driving Neural Induction.
750 *Cell Stem Cell* **25**, 713-727 e710, doi:10.1016/j.stem.2019.09.010 (2019).
751 31 Trevino, A. E. *et al.* Chromatin accessibility dynamics in a model of human forebrain
752 development. *Science* **367**, doi:10.1126/science.aay1645 (2020).
753 32 de la Torre-Ubieta, L. *et al.* The Dynamic Landscape of Open Chromatin during
754 Human Cortical Neurogenesis. *Cell* **172**, 289-304 e218,
755 doi:10.1016/j.cell.2017.12.014 (2018).
756 33 Inglis, G. A. S. *et al.* Transcriptomic and epigenomic dynamics associated with
757 development of human iPSC-derived GABAergic interneurons. *Hum Mol Genet* **29**,
758 2579-2595, doi:10.1093/hmg/ddaa150 (2020).
759 34 Ogiwara, I. *et al.* Nav1.1 localizes to axons of parvalbumin-positive inhibitory
760 interneurons: a circuit basis for epileptic seizures in mice carrying an Scn1a gene
761 mutation. *J Neurosci* **27**, 5903-5914, doi:10.1523/JNEUROSCI.5270-06.2007 (2007).
762 35 Maroof, A. M. *et al.* Directed differentiation and functional maturation of cortical
763 interneurons from human embryonic stem cells. *Cell Stem Cell* **12**, 559-572,
764 doi:10.1016/j.stem.2013.04.008

765 S1934-5909(13)00144-6 [pii] (2013).
766 36 Strano, A., Tuck, E., Stubbs, V. E. & Livesey, F. J. Variable Outcomes in Neural
767 Differentiation of Human PSCs Arise from Intrinsic Differences in Developmental
768 Signaling Pathways. *Cell Rep* **31**, doi:ARTN 107732

769 10.1016/j.celrep.2020.107732 (2020).
770 37 Stevanovic, M. *et al.* SOX Transcription Factors as Important Regulators of Neuronal
771 and Glial Differentiation During Nervous System Development and Adult
772 Neurogenesis. *Front Mol Neurosci* **14**, doi:ARTN 654031

773 10.3389/fnmol.2021.654031 (2021).

774 38 Lindtner, S. *et al.* Genomic Resolution of DLX-Orchestrated Transcriptional Circuits
775 Driving Development of Forebrain GABAergic Neurons. *Cell Rep* **28**, 2048-+,
776 doi:10.1016/j.celrep.2019.07.022 (2019).
777 39 Schep, A. N., Wu, B., Buenrostro, J. D. & Greenleaf, W. J. chromVAR: inferring
778 transcription-factor-associated accessibility from single-cell epigenomic data. *Nat*
779 *Methods* **14**, 975-978, doi:10.1038/nmeth.4401 (2017).
780 40 Brunklaus, A. *et al.* Time to move beyond genetics towards biomedical data-driven
781 translational genomic research in severe paediatric epilepsies. *Eur J Paediatr Neurol*
782 **24**, 35-39, doi:10.1016/j.ejpn.2019.12.001 (2020).
783 41 Brunklaus, A. *et al.* SCN1A variants from bench to bedside-improved clinical
784 prediction from functional characterization. *Hum Mutat* **41**, 363-374,
785 doi:10.1002/humu.23943 (2020).
786 42 Liu, Y. *et al.* Dravet syndrome patient-derived neurons suggest a novel epilepsy
787 mechanism. *Ann Neurol* **74**, 128-139, doi:10.1002/ana.23897 (2013).
788 43 Inoue, Y. *et al.* Stiripentol open study in Japanese patients with Dravet syndrome.
789 *Epilepsia* **50**, 2362-2368, doi:10.1111/j.1528-1167.2009.02179.x (2009).
790 44 Dressler, A. *et al.* Efficacy and tolerability of the ketogenic diet in Dravet syndrome -
791 Comparison with various standard antiepileptic drug regimen. *Epilepsy Res* **109**, 81-
792 89, doi:10.1016/j.eplepsyres.2014.10.014 (2015).
793 45 Baumann, C., Zhang, X., Zhu, L., Fan, Y. & De La Fuente, R. Changes in chromatin
794 accessibility landscape and histone H3 core acetylation during valproic acid-induced
795 differentiation of embryonic stem cells. *Epigenetics Chromatin* **14**, 58,
796 doi:10.1186/s13072-021-00432-5 (2021).
797 46 Stevanovic, M. *et al.* SOX Transcription Factors as Important Regulators of Neuronal
798 and Glial Differentiation During Nervous System Development and Adult
799 Neurogenesis. *Front Mol Neurosci* **14**, 654031, doi:10.3389/fnmol.2021.654031
800 (2021).
801 47 Sobol, M. *et al.* Methods of Reprogramming to Induced Pluripotent Stem Cell
802 Associated with Chromosomal Integrity and Delineation of a Chromosome 5q
803 Candidate Region for Growth Advantage. *Stem Cells Dev* **24**, 2032-2040,
804 doi:10.1089/scd.2015.0061 (2015).
805 48 Chen, X. *et al.* ATAC-see reveals the accessible genome by transposase-mediated
806 imaging and sequencing. *Nat Methods* **13**, 1013-1020, doi:10.1038/nmeth.4031

807 nmeth.4031 [pii] (2016).
808 49 Buenrostro, J. D., Giresi, P. G., Zaba, L. C., Chang, H. Y. & Greenleaf, W. J.
809 Transposition of native chromatin for fast and sensitive epigenomic profiling of open
810 chromatin, DNA-binding proteins and nucleosome position. *Nat Methods* **10**, 1213-
811 1218, doi:10.1038/nmeth.2688 (2013).
812 50 Langmead, B., Trapnell, C., Pop, M. & Salzberg, S. L. Ultrafast and memory-efficient
813 alignment of short DNA sequences to the human genome. *Genome Biol* **10**, R25,
814 doi:10.1186/gb-2009-10-3-r25 (2009).
815 51 Zhang, Y. *et al.* Model-based analysis of ChIP-Seq (MACS). *Genome Biol* **9**, R137,
816 doi:10.1186/gb-2008-9-9-r137 (2008).
817 52 Ramirez, F., Dundar, F., Diehl, S., Gruning, B. A. & Manke, T. deepTools: a flexible
818 platform for exploring deep-sequencing data. *Nucleic Acids Res* **42**, W187-191,
819 doi:10.1093/nar/gku365 (2014).
820 53 Robinson, M. D., McCarthy, D. J. & Smyth, G. K. edgeR: a Bioconductor package for
821 differential expression analysis of digital gene expression data. *Bioinformatics* **26**,
822 139-140, doi:10.1093/bioinformatics/btp616 (2010).
823 54 Love, M. I., Huber, W. & Anders, S. Moderated estimation of fold change and
824 dispersion for RNA-seq data with DESeq2. *Genome Biol* **15**, 550,
825 doi:10.1186/s13059-014-0550-8 (2014).
826 55 Futschik M, C. B. Noise robust clustering of gene expression time-course data.
827 *Journal of Bioinformatics and Computational Biology*, 965-988 (2005).
828 56 Yu, G., Wang, L. G. & He, Q. Y. ChIPseeker: an R/Bioconductor package for ChIP
829 peak annotation, comparison and visualization. *Bioinformatics* **31**, 2382-2383,
830 doi:10.1093/bioinformatics/btv145 (2015).
831 57 Yu, G. C., Wang, L. G., Han, Y. Y. & He, Q. Y. clusterProfiler: an R Package for
832 Comparing Biological Themes Among Gene Clusters. *Omics* **16**, 284-287,
833 doi:10.1089/omi.2011.0118 (2012).
834 58 Heinz, S. *et al.* Simple combinations of lineage-determining transcription factors
835 prime cis-regulatory elements required for macrophage and B cell identities. *Mol Cell*
836 **38**, 576-589, doi:10.1016/j.molcel.2010.05.004 (2010).

837

838

839 **Figure legends:**

840 **Main figures:**

841 **Figure 1: Chromatin accessibility dynamics during GABAeric interneuron differentiation**
842 **of control iPSCs**

843 **A.** Schematic illustration of GABAergic interneuron differentiation protocol. Cells from
844 iPSC differentiation were collected for ATAC-Seq. Interneuron differentiation was
845 grouped into four stages: iPSC (Day 0), neural progenitor cells; NPCs (Day 19),
846 immature neurons, imN (Day 35), GABAergic interneurons, GABA (Day 65).

847 **B.** Heatmap of four Clusters identified by time series analysis using temporal changes in
848 chromatin accessibility compared to D0 (Day 0) and other points. The signal strengths
849 were denoted by color intensities.

850 **C.** Line plots showing chromatin accessibility at cluster-specific regions from each time
851 point.

852 **D.** Barplot for genomic distribution of differential chromatin accessible regions for each
853 cluster.

854 **E.** Heatmap for top 10 TFs enrichment in each cluster. The significance was denoted by
855 color intensities. O-S-E-N = OCT4-SOX2-TCF-NANOG.

856 **F.** Bubble plot of KEGG pathway enrichment for each cluster. p-value and enrichment
857 were indicated. The corresponding comprehensive list of enrichment terms can be found
858 in Supplementary Table 2.

859 **G.** Genome browser view showing representative differential chromatin accessible regions
860 at the indicated gene loci. Additionally, RNA-seq data[13] is visualized at D19 and D65.

861

862

863

864 **Figure 2: Chromatin accessibility dynamics during GABAergic differentiation of Dravet**
865 **Syndrome patient iPSCs**

866 **A.** Schematic Illustration of the design for GABAergic differentiation in Dravet syndrome
867 patients. Cells from iPSC differentiation were collected for ATAC-Seq. GABAergic
868 differentiation in Dravet Syndrome patients was grouped into four stages: iPSC (Day 0),
869 NPCs (Day 19), imN (Day 35), GABA(Day 65).

870 **B.** Heatmap of four clusters identified by time series analysis using temporal changes in
871 chromatin accessibility compared D0 (Day 0) and other points. The signal strengths
872 were denoted by color intensities

873 **C.** Line plots showing chromatin accessibility at cluster-specific regions from each time
874 point.
875 **D.** Barplot for genomic distribution of differential chromatin accessible regions for each
876 cluster.
877 **E.** Heatmap for top 10 TFs enrichment in each cluster. The significance was denoted by
878 color intensities. O-S-E-N = OCT4-SOX2-TCF-NANOG.
879 **F.** Bubble plot of KEGG pathway enrichment for each cluster. p-value and enrichment
880 were indicated. The corresponding comprehensive list of enrichment terms can be found
881 in Supplementary Table 4.
882 **G.** Genome browser view showing representative differential chromatin accessible regions
883 at the indicated gene loci. Additionally, RNA-seq data[13] is visualized at D19 and D65.
884
885
886
887 **Figure 3: Common chromatin accessibility features of control and Dravet Syndrome**
888 **patient iPSCs during GABAergic differentiation**
889
890 **A.** Heatmap for common chromatin accessible regions detected between control and
891 Dravet Syndrome (DS) group during differentiation. Four clusters were obtained from
892 time series analysis. Representative genes are labeled on the right side of heatmap.
893 **B.** Barplot for genomic distribution of chromatin accessible regions for each cluster.
894 **C.** Bubble plot of KEGG pathway enrichment for each cluster. p-value and enrichment
895 were indicated.
896 **D.** Genome browser view showing representative chromatin accessible regions at the
897 indicated gene loci. These genes represent common changing regions between control
898 and patients groups.
899 **E.** Transcription factors (TFs) deviation Z scores heatmap for unique TF enriched in each
900 cluster. Representative TFs are labeled on the right side of heatmap.
901 **F.** Representative TFs enrichment (deviation Z score) dynamics at ATAC-Seq peaks in
902 control and Dravet Syndrome (DS) group during differentiation.
903
904 **Figure 4: Unique chromatin accessibility features of control and Dravet Syndrome patient**
905 **iPSCs during GABAergic differentiation**

906 **A.** Principal component analysis (PCA) plot of all ATAC-Seq from control and Dravet
907 Syndrome patients during GABAergic differentiation.
908 **B.** Heatmap showing the differential chromatin accessible peaks for comparison at each
909 time point between the control and Dravet Syndrome (DS) patients. Representative
910 genes are labeled on the right side of heatmap.
911 **C.** Barplot for genomic features of unique chromatin accessible regions at each time point
912 for the control and Dravet Syndrome (DS) patients.
913 **D.** Bubble plot of KEGG pathway enrichment at GABAeric interneuron (Day 65) for the
914 control and Dravet Syndrome (DS) patients. p-value and enrichment score were
915 indicated.
916 **E.** Heatmap showing transcription factors (TFs) enrichment at differential chromatin
917 accessible peaks for comparison at each time point between the control and Dravet
918 Syndrome (DS) patients. Representative TFs are labeled on the right side of heatmap.
919 **F.** Representative TFs enrichment (deviation Z score) dynamics at ATAC-Seq peaks in
920 control and Dravet Syndrome (DS) group during differentiation.
921
922 **Figure 5: Chromatin accessibility response to Valproic acid treatment in GABAergic**
923 **interneurons**
924 **A.** Schematic illustration showing measurement of chromatin accessibility response in
925 valproic acid (VPA) treatment of GABAergic interneurons.
926 **B.** Principal component analysis (PCA) plot of ATAC-Seq with and without VPA
927 treatment of GABAergic interneuron in control and Dravet Syndrome patients.
928 **C.** Heatmap of differential chromatin accessible peaks from the VPA responsible group,
929 consisting of two control samples and one Dravet Syndrome (DS) patient sample.
930 **D.** Barplot for genomic distribution of VPA responsible accessible regions from
931 differential conditions.
932 **E.** Bubble plot of KEGG pathway enrichment for each condition. p-value and enrichment
933 were indicated.
934 **F.** TF deviation Z score heatmap for top 50 transcription factors (TFs) enriched at
935 responsible chromatin regions from differential conditions.
936 **G.** Genome browser view showing representative VPA responsible chromatin accessible
937 regions at the indicated gene loci.
938

# Figure 1

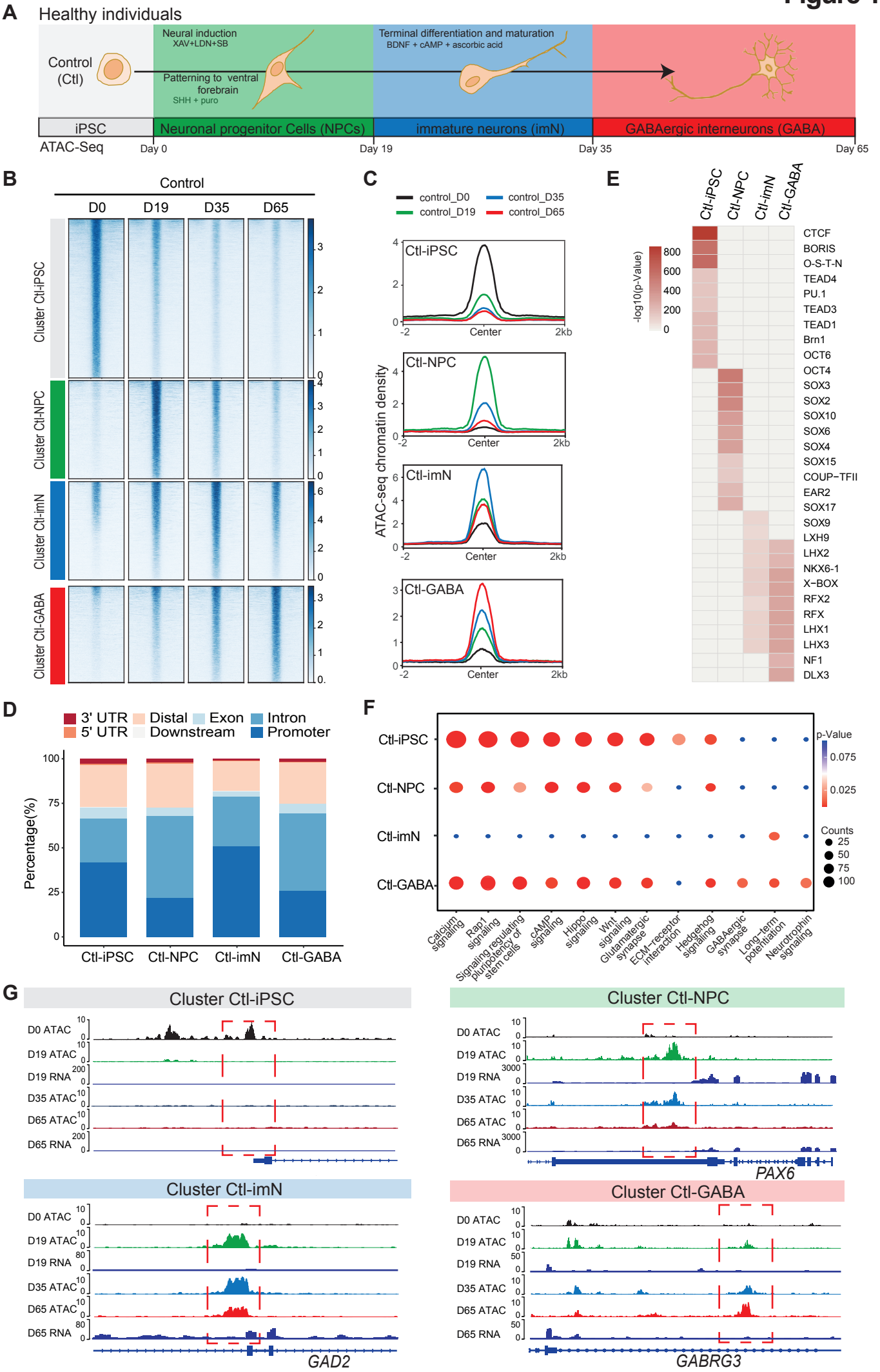
A
Healthy individuals
Control (Ctl)
Neural induction
XAV+LDN+SB
Patterning to ventral forebrain
SHH + puro
Terminal differentiation and maturation
BDNF + cAMP + ascorbic acid
iPSC
Neuronal progenitor Cells (NPCs)
immature neurons (imN)
GABAergic interneurons (GABA)
ATAC-Seq
Day 0
Day 19
Day 35
Day 65
B
Control
D0
D19
D35
D65
Cluster Ctl-iPSC
Cluster Ctl-NPC
Cluster Ctl-imN
Cluster Ctl-GABA
C
control_D0
control_D19
control_D35
control_D65
Ctl-iPSC
Ctl-NPC
Ctl-imN
Ctl-GABA
ATAC-seq chromatin density
Center
2kb
E
Ctl-iPSC
Ctl-NPC
Ctl-imN
Ctl-GABA
-log10(p-Value)
CTCF
BORIS
O-S-T-N
TEAD4
PU.1
TEAD3
TEAD1
Brn1
OCT6
OCT4
SOX3
SOX2
SOX10
SOX6
SOX4
SOX15
COUP-TFII
EAR2
SOX17
SOX9
LXH9
LHX2
NKX6-1
X-BOX
RFX2
RFX
LHX1
LHX3
NF1
DLX3
D
3' UTR
5' UTR
Distal
Downstream
Exon
Intron
Promoter
Percentage(%)
Ctl-iPSC
Ctl-NPC
Ctl-imN
Ctl-GABA
F
p-Value
Counts
Calcium signaling
Rap1 signaling
Signaling regulating pluripotency of stem cells
cAMP signaling
Hippo signaling
Wnt signaling
Glutamatergic synapse
ECM-receptor interaction
Hedgehog signaling
GABAergic synapse
Long-term potentiation
Neurotrophin signaling
G
Cluster Ctl-iPSC
Cluster Ctl-NPC
Cluster Ctl-imN
Cluster Ctl-GABA
D0 ATAC
D19 ATAC
D19 RNA
D35 ATAC
D65 ATAC
D65 RNA
PAX6
GAD2
GABRG3

# Figure 2

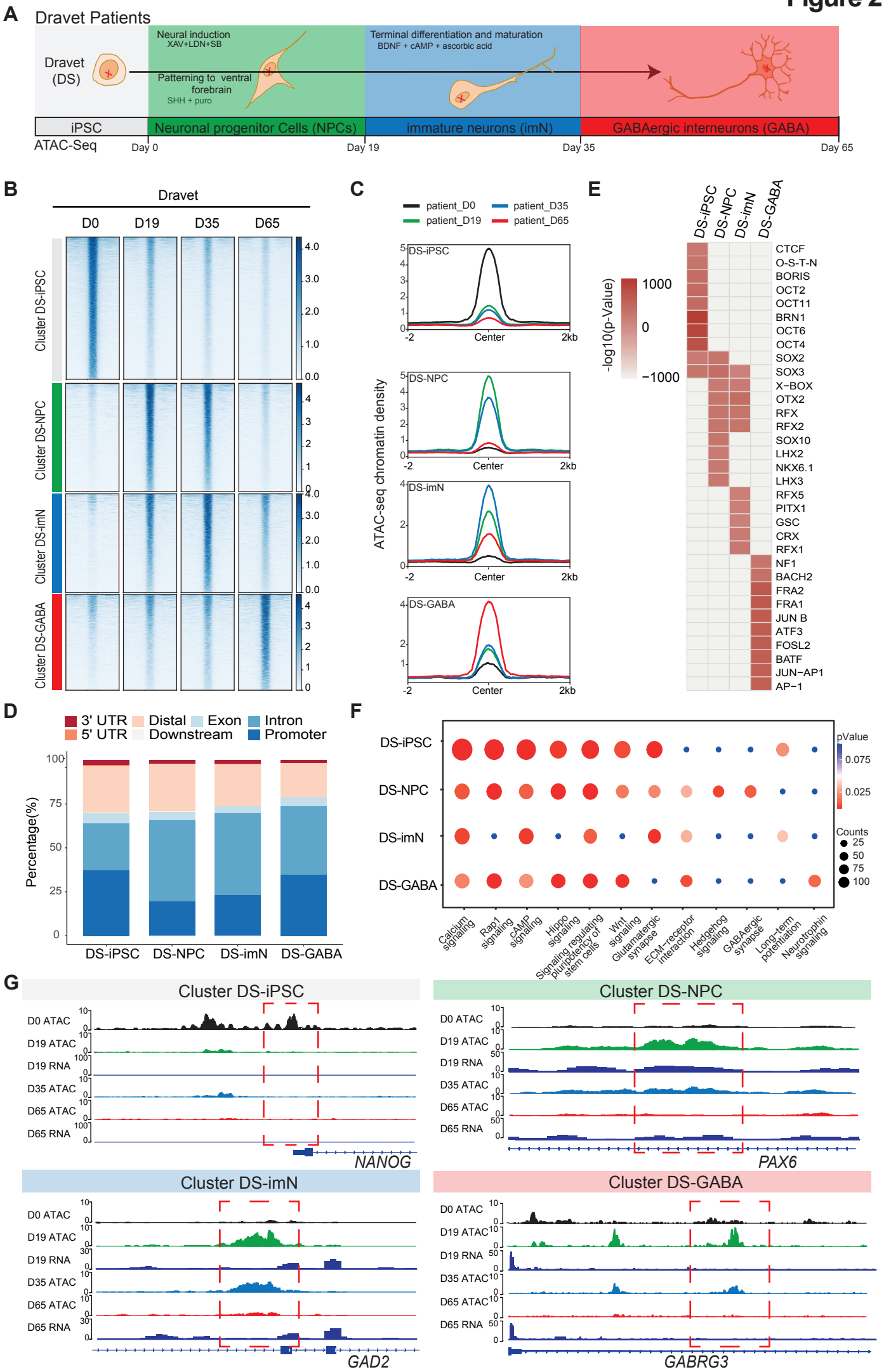
A
Dravet Patients
Dravet (DS)
Neural induction
XAV+LDN+SB
Patterning to ventral forebrain
SHH + puro
Terminal differentiation and maturation
BDNF + cAMP + ascorbic acid
iPSC
ATAC-Seq
Neuronal progenitor Cells (NPCs)
immature neurons (imN)
GABAergic interneurons (GABA)
Day 0
Day 19
Day 35
Day 65
B
Dravet
D0
D19
D35
D65
Cluster DS-iPSC
Cluster DS-NPC
Cluster DS-imN
Cluster DS-GABA
C
patient_D0
patient_D19
patient_D35
patient_D65
DS-iPSC
DS-NPC
DS-imN
DS-GABA
ATAC-seq chromatin density
Center
2kb
E
DS-iPSC
DS-NPC
DS-imN
DS-GABA
-log10(p-Value)
1000
0
−1000
CTCF
O-S-T-N
BORIS
OCT2
OCT11
BRN1
OCT6
OCT4
SOX2
SOX3
X−BOX
OTX2
RFX
RFX2
SOX10
LHX2
NKX6.1
LHX3
RFX5
PITX1
GSC
CRX
RFX1
NF1
BACH2
FRA2
FRA1
JUN B
ATF3
FOSL2
BATF
JUN−AP1
AP−1
D
3' UTR
5' UTR
Distal
Downstream
Exon
Intron
Promoter
Percentage(%)
DS-iPSC
DS-NPC
DS-imN
DS-GABA
F
DS-iPSC
DS-NPC
DS-imN
DS-GABA
pValue
0.075
0.025
Counts
25
50
75
100
Calcium signaling
Rap1 signaling
cAMP signaling
Hippo signaling
Signaling regulating pluripotency of stem cells
Wnt signaling
Glutamatergic synapse
ECM−receptor interaction
Hedgehog signaling
GABAergic synapse
Long-term potentiation
Neurotrophin signaling
G
Cluster DS-iPSC
D0 ATAC
D19 ATAC
D19 RNA
D35 ATAC
D65 ATAC
D65 RNA
NANOG
Cluster DS-NPC
PAX6
Cluster DS-imN
GAD2
Cluster DS-GABA
GABRG3

# Figure 3

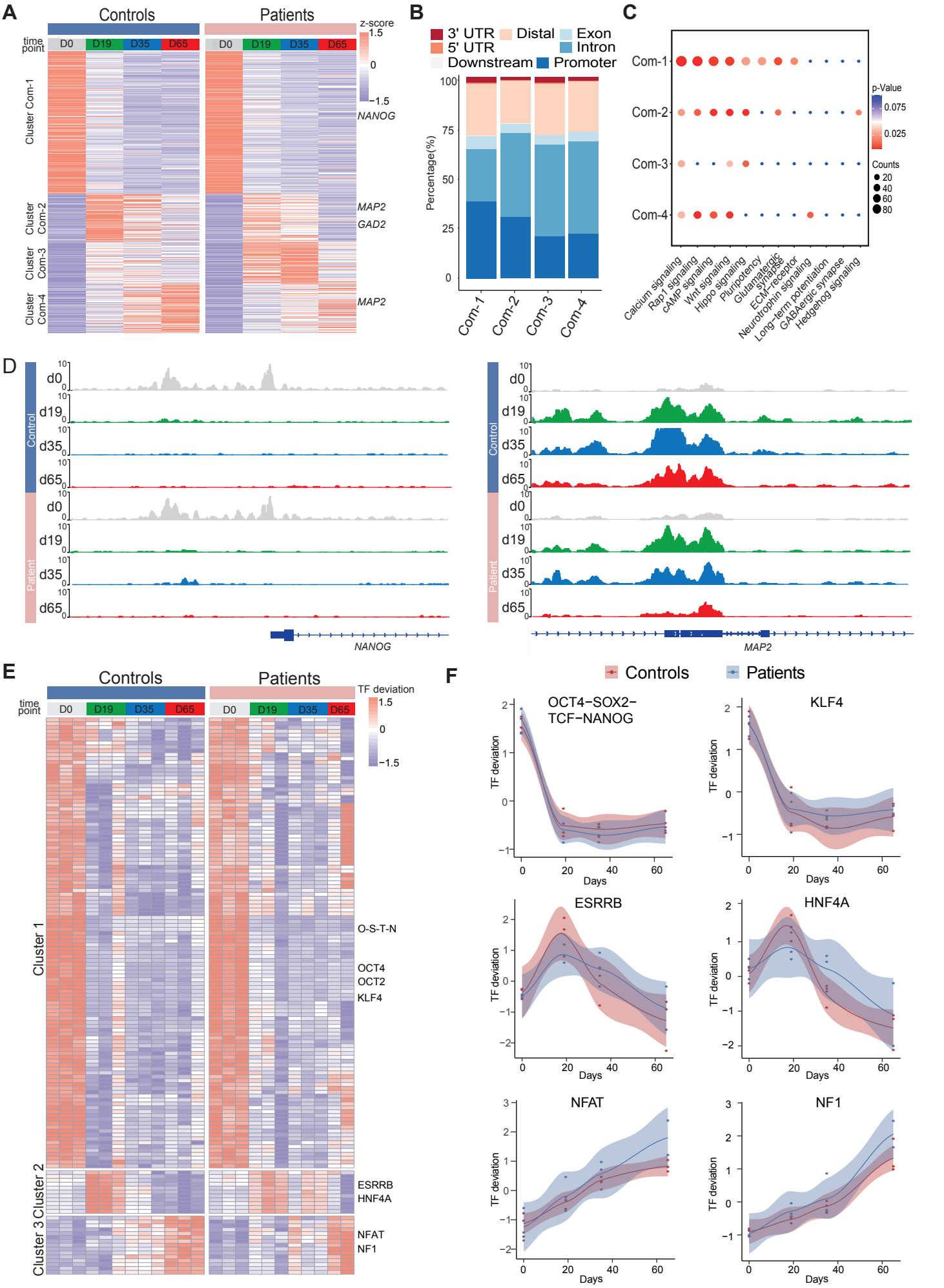
A
Controls
Patients
time point
D0
D19
D35
D65
z-score
1.5
0
−1.5
Cluster Com-1
Cluster Com-2
Cluster Com-3
Cluster Com-4
NANOG
MAP2
GAD2
MAP2
B
3' UTR
5' UTR
Distal
Downstream
Exon
Intron
Promoter
Percentage(%)
100
75
50
25
0
Com-1
Com-2
Com-3
Com-4
C
Com-1
Com-2
Com-3
Com-4
p-Value
0.075
0.025
Counts
20
40
60
80
Calcium signaling
Rap1 signaling
cAMP signaling
Wnt signaling
Hippo signaling
Pluripotency
Glutamatergic synapse
ECM−receptor
Neurotrophin signaling
Long−term potentiation
GABAergic synapse
Hedgehog signaling
D
Control
Patient
d0
d19
d35
d65
NANOG
MAP2
E
Controls
Patients
time point
D0
D19
D35
D65
TF deviation
1.5
0
−1.5
Cluster 1
Cluster 2
Cluster 3
O-S-T-N
OCT4
OCT2
KLF4
ESRRB
HNF4A
NFAT
NF1
F
Controls
Patients
OCT4−SOX2−TCF−NANOG
KLF4
ESRRB
HNF4A
NFAT
NF1
TF deviation
Days

# Figure 4

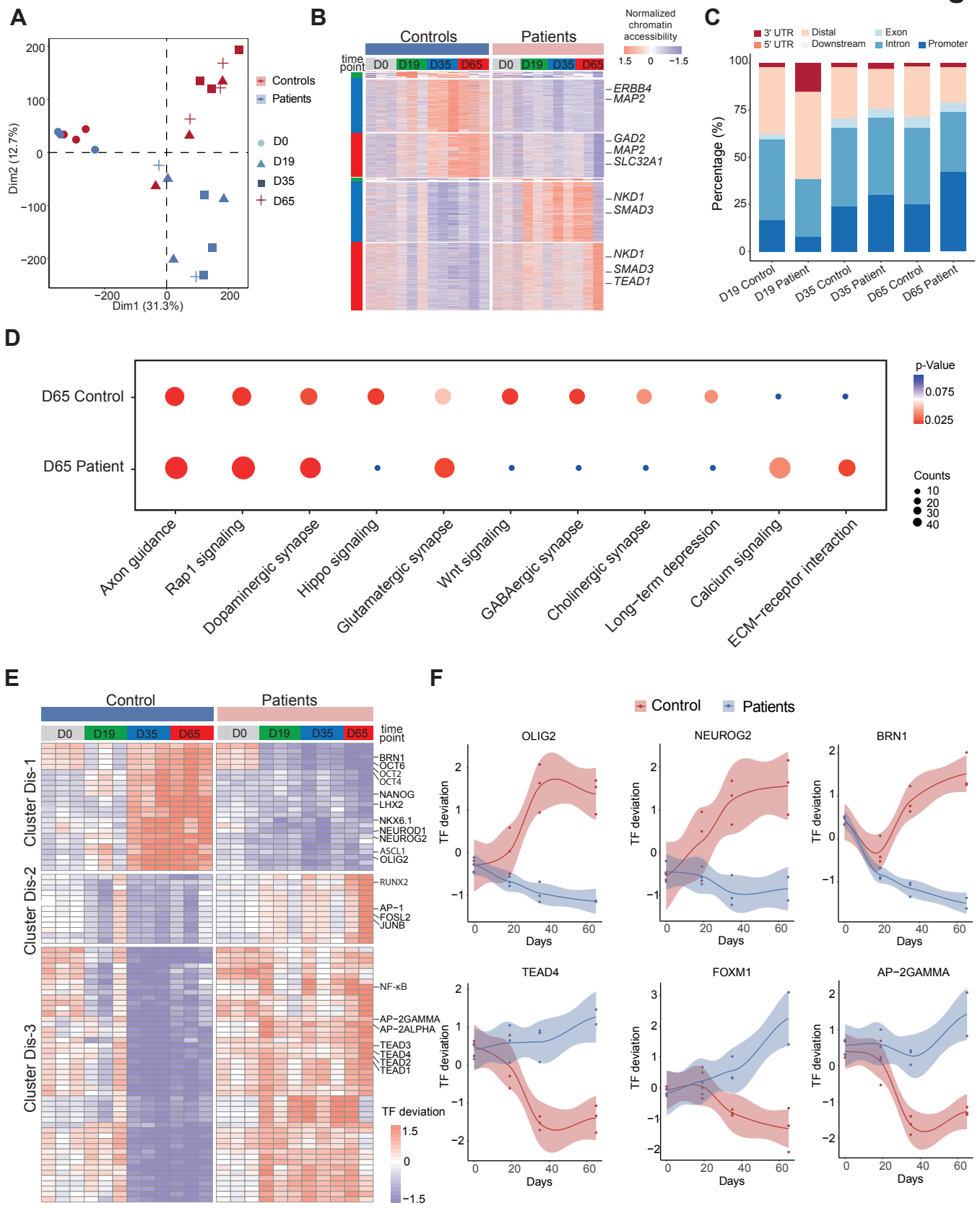
A
Dim2 (12.7%)
Dim1 (31.3%)
Controls
Patients
D0
D19
D35
D65
B
Controls
Patients
time point
D0 D19 D35 D65
Normalized chromatin accessibility
1.5 0 −1.5
ERBB4
MAP2
GAD2
MAP2
SLC32A1
NKD1
SMAD3
NKD1
SMAD3
TEAD1
C
3' UTR
5' UTR
Distal
Downstream
Exon
Intron
Promoter
Percentage (%)
D19 Control
D19 Patient
D35 Control
D35 Patient
D65 Control
D65 Patient
D
D65 Control
D65 Patient
p-Value
0.075
0.025
Counts
10
20
30
40
Axon guidance
Rap1 signaling
Dopaminergic synapse
Hippo signaling
Glutamatergic synapse
Wnt signaling
GABAergic synapse
Cholinergic synapse
Long−term depression
Calcium signaling
ECM−receptor interaction
E
Control
Patients
D0 D19 D35 D65
time point
Cluster Dis-1
Cluster Dis-2
Cluster Dis-3
BRN1
OCT6
OCT2
OCT4
NANOG
LHX2
NKX6.1
NEUROD1
NEUROG2
ASCL1
OLIG2
RUNX2
AP−1
FOSL2
JUNB
NF-κB
AP−2GAMMA
AP−2ALPHA
TEAD3
TEAD4
TEAD2
TEAD1
TF deviation
1.5
0
−1.5
F
Control
Patients
OLIG2
NEUROG2
BRN1
TEAD4
FOXM1
AP−2GAMMA
TF deviation
Days

# Figure 5

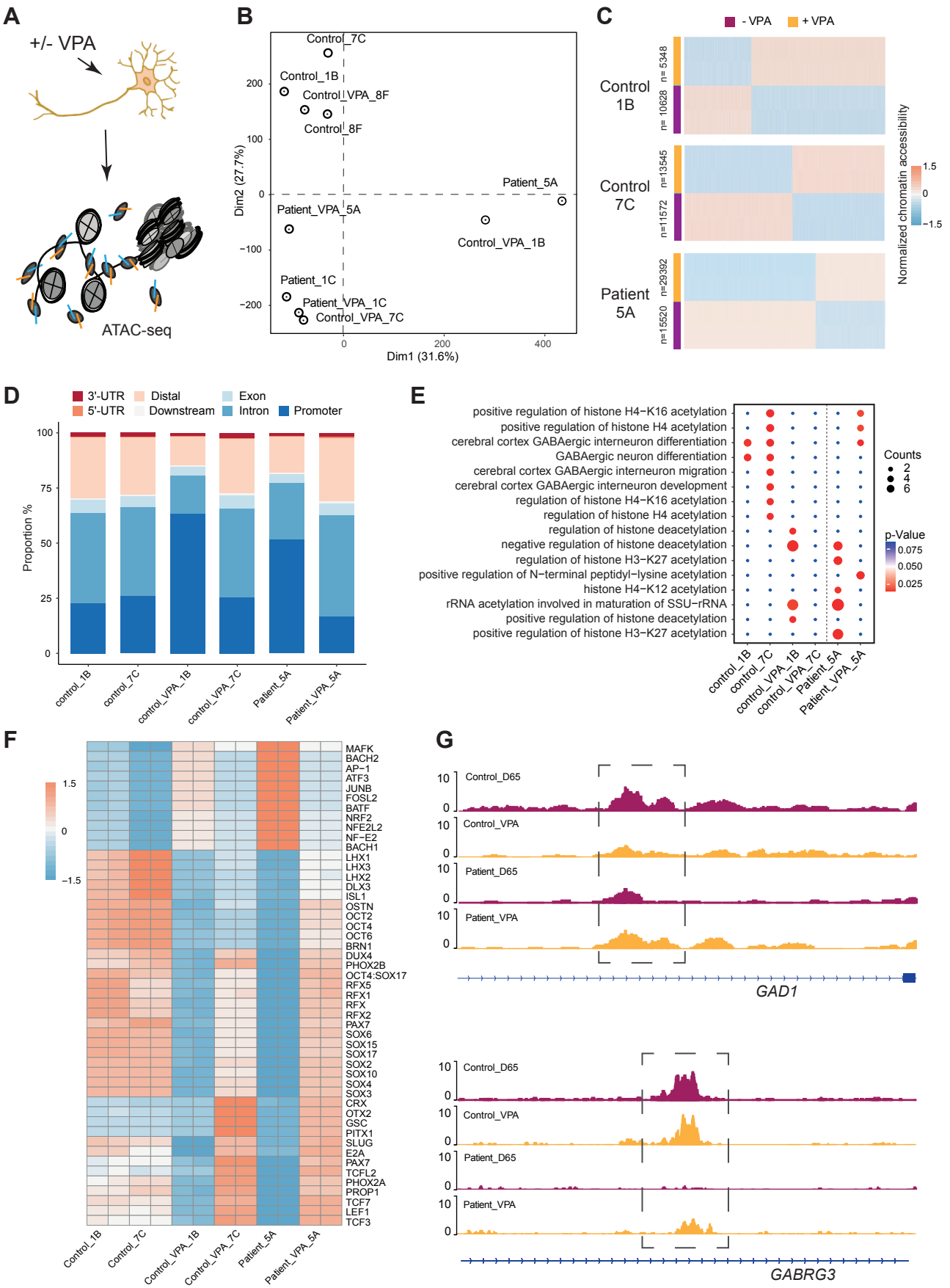
A
+/- VPA
ATAC-seq
B
Control_7C
Control_1B
Control_VPA_8F
Control_8F
Patient_5A
Patient_VPA_5A
Control_VPA_1B
Patient_1C
Patient_VPA_1C
Control_VPA_7C
Dim2 (27.7%)
Dim1 (31.6%)
C
- VPA
+ VPA
Control 1B
Control 7C
Patient 5A
n= 5348
n= 10628
n=13545
n=11572
n=29392
n=15520
Normalized chromatin accessibility
D
3'-UTR
5'-UTR
Distal
Downstream
Exon
Intron
Promoter
Proportion %
control_1B
control_7C
control_VPA_1B
control_VPA_7C
Patient_5A
Patient_VPA_5A
E
positive regulation of histone H4−K16 acetylation
positive regulation of histone H4 acetylation
cerebral cortex GABAergic interneuron differentiation
GABAergic neuron differentiation
cerebral cortex GABAergic interneuron migration
cerebral cortex GABAergic interneuron development
regulation of histone H4−K16 acetylation
regulation of histone H4 acetylation
regulation of histone deacetylation
negative regulation of histone deacetylation
regulation of histone H3−K27 acetylation
positive regulation of N−terminal peptidyl−lysine acetylation
histone H4−K12 acetylation
rRNA acetylation involved in maturation of SSU−rRNA
positive regulation of histone deacetylation
positive regulation of histone H3−K27 acetylation
Counts
p-Value
F
MAFK
BACH2
AP−1
ATF3
JUNB
FOSL2
BATF
NRF2
NFE2L2
NF−E2
BACH1
LHX1
LHX3
LHX2
DLX3
ISL1
OSTN
OCT2
OCT4
OCT6
BRN1
DUX4
PHOX2B
OCT4:SOX17
RFX5
RFX1
RFX
RFX2
PAX7
SOX6
SOX15
SOX17
SOX2
SOX10
SOX4
SOX3
CRX
OTX2
GSC
PITX1
SLUG
E2A
PAX7
TCFL2
PHOX2A
PROP1
TCF7
LEF1
TCF3
G
Control_D65
Control_VPA
Patient_D65
Patient_VPA
GAD1
GABRG3

## Supplementary Figures 1-8:

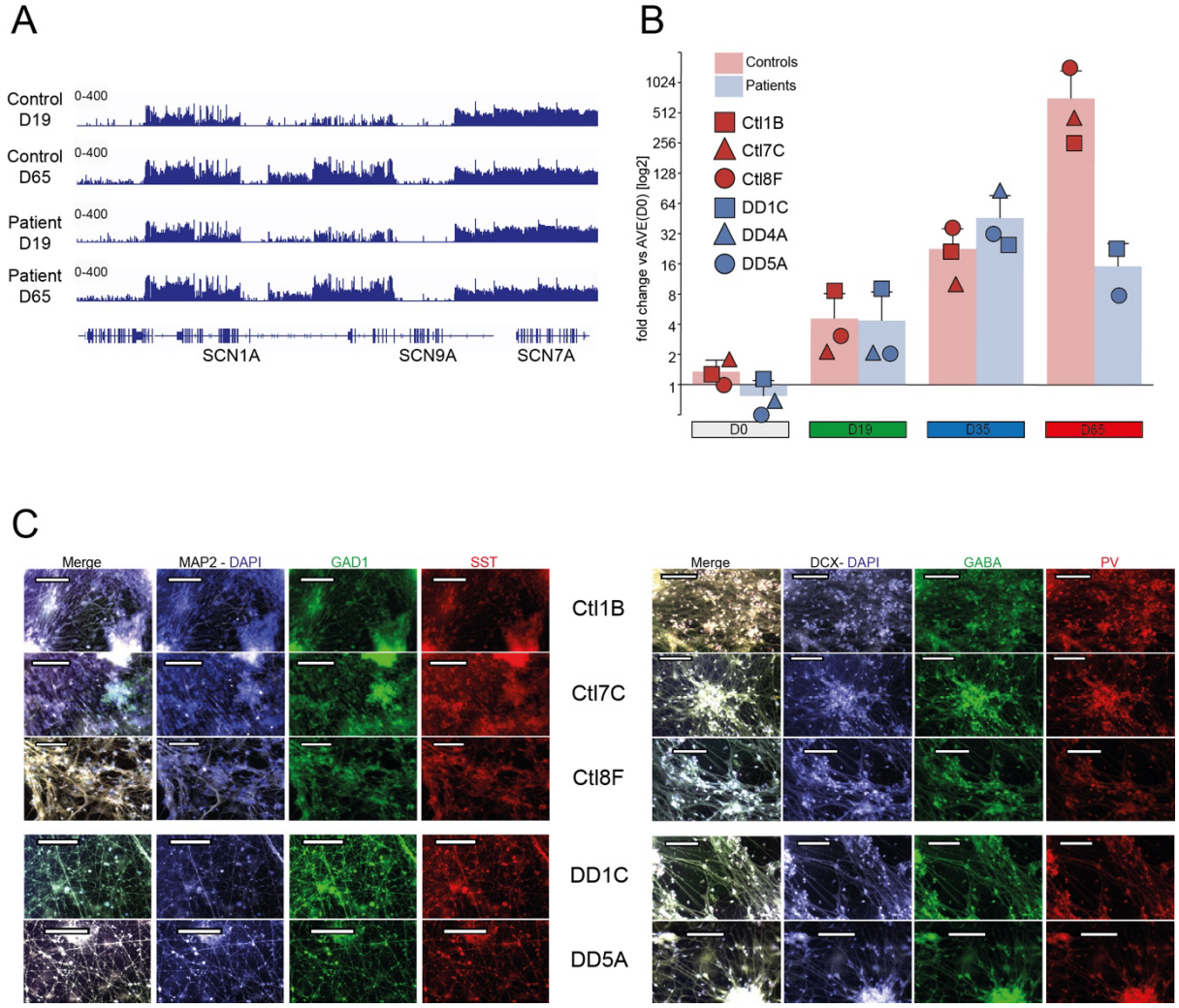


**Supplementary Figure 1: validation of GABAergic differentiation.**

- **A.** *SCN1A* gene expression at day 19 and day 65 from RNAseq.
- **B.** *SCN1A* expression levels quantified by qRT-PCR following GABAergic differentiation of control and patient iPSC relative to expression of the housekeeping genes ACTB and GAPDH at D0, D19, D35 and D65. Fold change data are presented as log2 [mean ΔΔCT(day Y)] ± SD and individual data points for each cell line are indicated (Control lines in red: Ctl1B - square, Ctl7C - triangle, Ctl8F – circle; patient lines in blue: DD1C - square, DD4A - triangle, DD5A – circle; please see Methods for detail). Ctl1B, Ctl7C, Ctl8F, DD1C, DD4A, DD5A are names of cell lines.
- **C.** Representative pictures of immunofluorescent staining of Ctl-iPSC and DS-iPSC derived GABAergic neurons at D65 (Ctl-GABA) of GABAergic interneuron differentiation. The GABA cells form networks and stain positive for the neuronal markers MAP2 and double cortin (DCX), the GABAergic marker γ-aminobutyric acid (GABA) and the interneuronal markers somatostatin (SST), parvalbumin (PV) and glutamate decarboxylase 1 (GAD1). Size bar 100 µm.

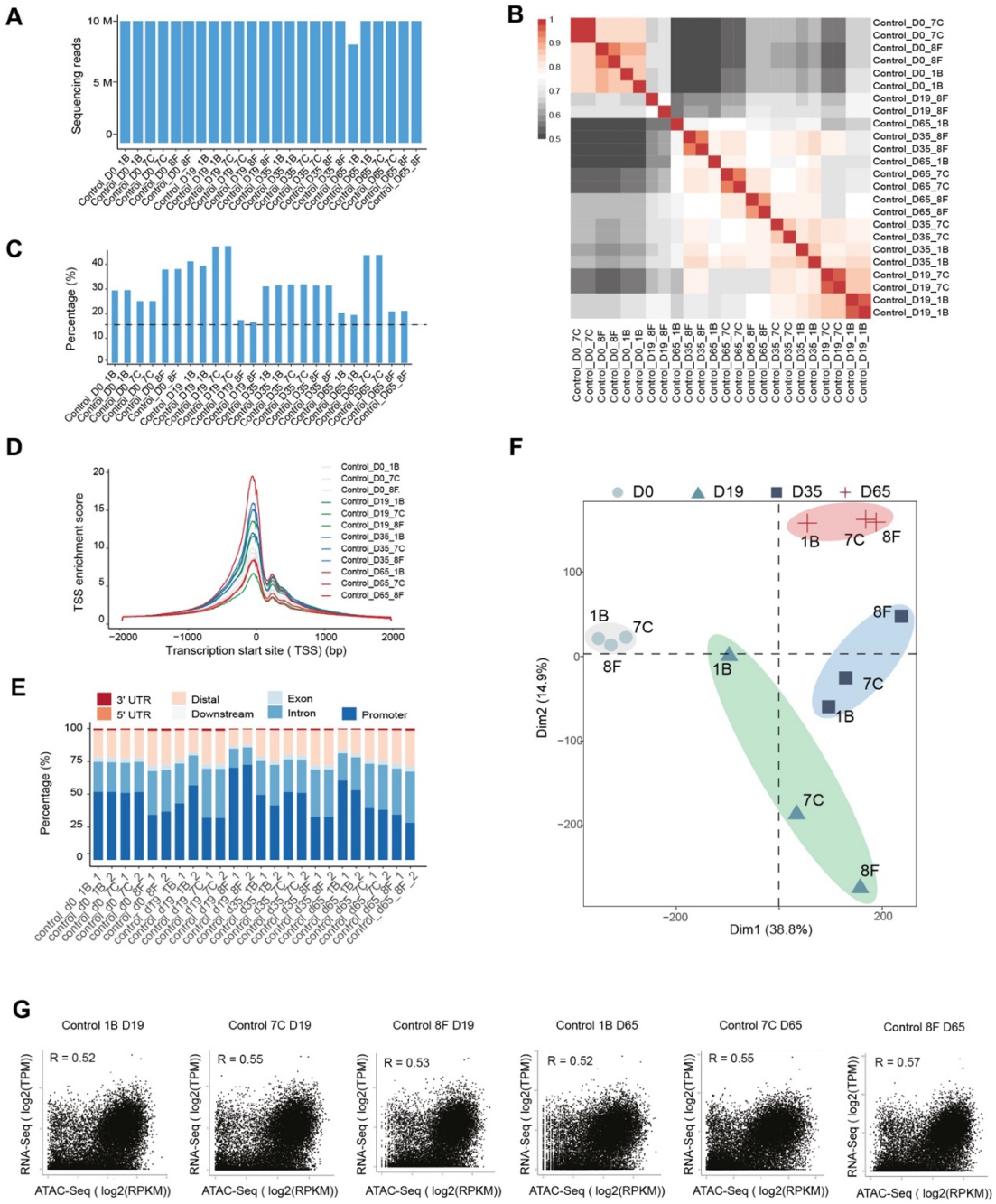


**Supplementary Figure 2: Quality control of ATAC-Seq samples during GABAergic interneuron differentiation of Ctl-iPSC.**

- **A.** Sequencing depth for each sample.
- **B.** Pearson correlation matrix from technical duplicates of ATAC-Seq at different time points.
- **C.** Quantification of fraction of reads in peaks (FRiP) of ATAC-Seq in each condition. The dotted line indicates the cutoff used.
- **D.** Transcription start site (TSS) enrichment score of ATAC-Seq in each sample.
- **E.** Genomic distribution of chromatin accessible peaks for each sample.
- **F.** Principal component analysis of ATAC-Seq from each sample.
- **G.** Pearson correlation of gene expression from RNA-Seq and chromatin accessibility from ATAC-Seq.

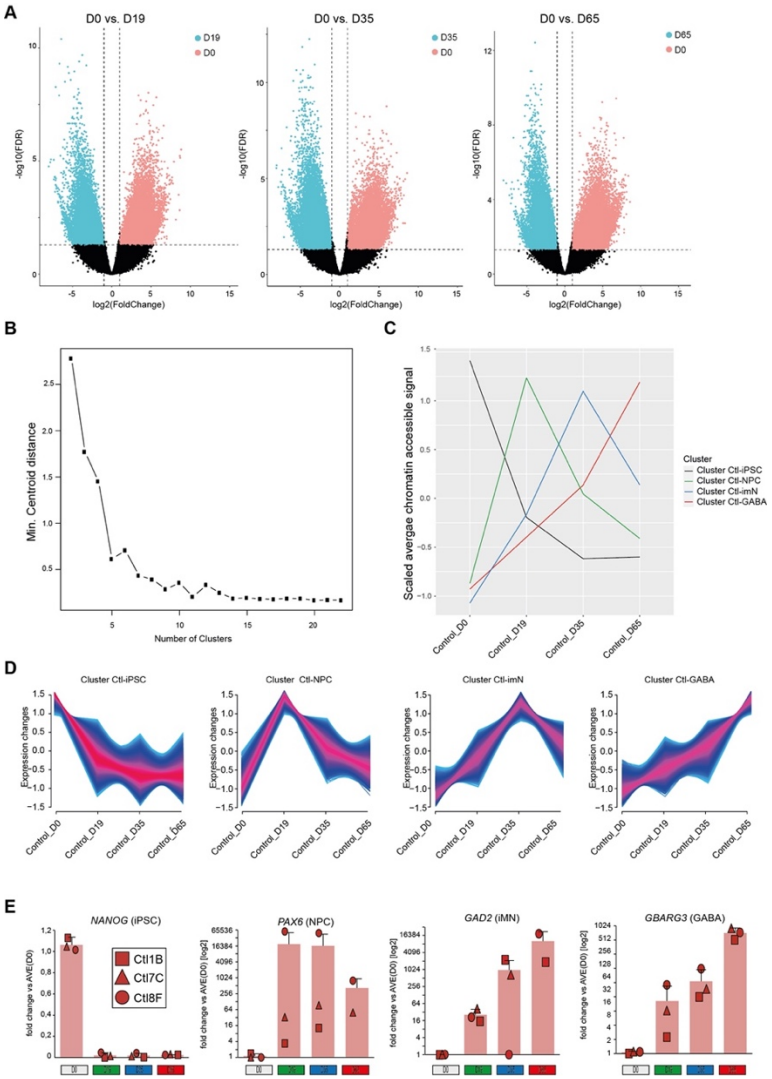


**Supplementary Figure 3: Chromatin accessibility cluster identification during GABAergic interneuron differentiation of Ctl-iPSC.**

- **A.** Volcano plots show differential accessible chromatin peaks between D0 and different time points. D0 (n = 6046) vs. D19 (n = 3866); D0 (n = 8880) vs. D35 (n = 7865); D0 (n = 7870) vs. D65 (n = 7776). The dotted lines indicate the cutoff used to identify differential ATAC-Seq peaks.
- **B.** Variance with different numbers of clusters derived from chromatin accessibility during GABAergic interneuron differentiation
- **C.** The scaled average chromatin accessibility during GABAergic interneuron differentiation from each cluster.
- **D.** The tendency of chromatin accessibility during GABAergic interneuron differentiation from each cluster.
- **E.** Expression of the four cluster markers *NANOG* (iPSC; D0), *PAX6* (PNC; D19), *GAD2* (imN; D35) and *BABRG3* (GABA; D65) quantified by qRT-PCR following GABAergic differentiation of control iPSC relative to expression of the housekeeping genes ACTB and GAPDH. Fold change data are presented as log2 [mean ΔΔCT(day Y)] ± SD and individual data points for each cell line are indicated (Control lines in red: Ctl1B - square, Ctl7C - triangle, Ctl8F – circle please see Methods for detail).

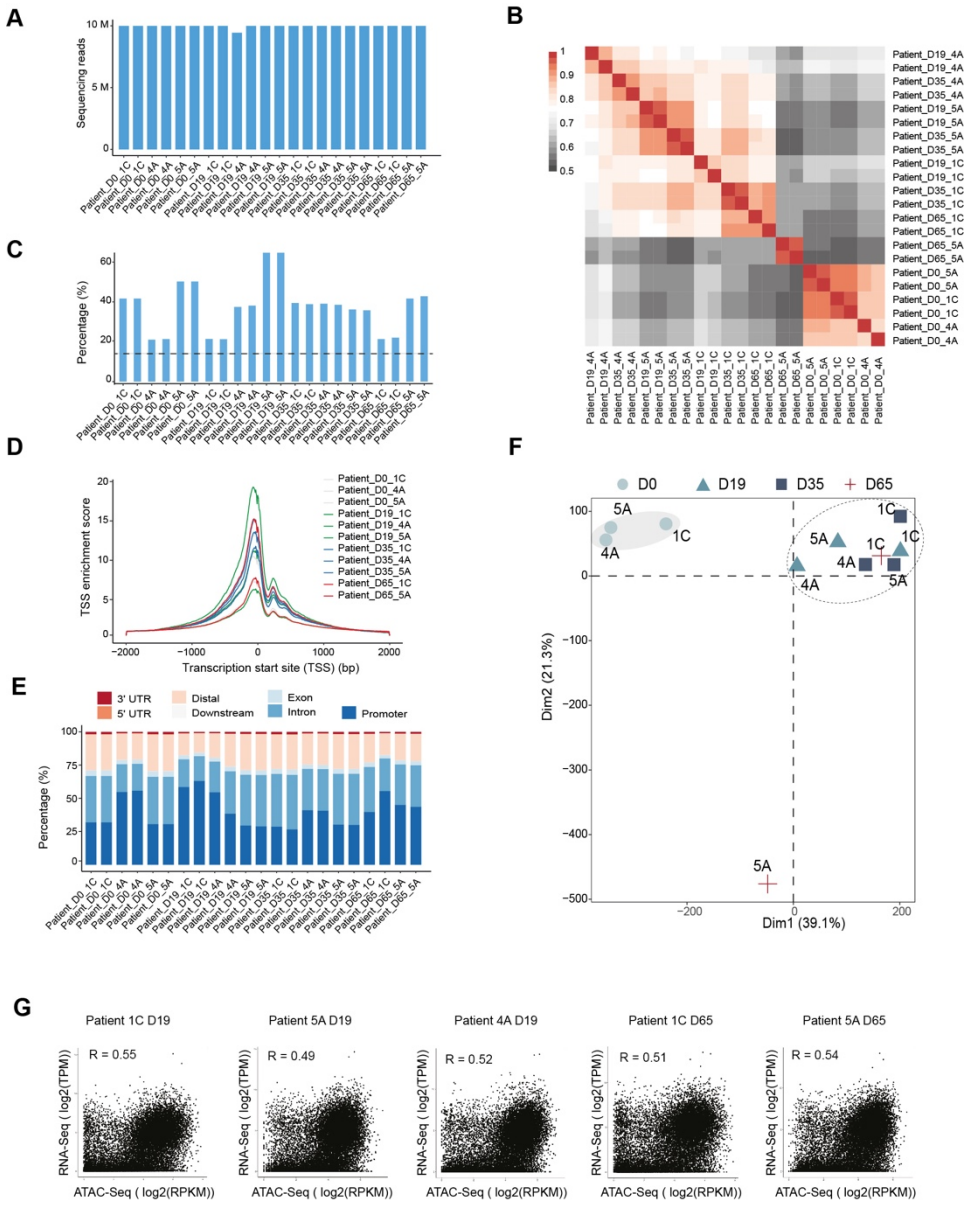


**Supplementary Figure 4: Quality control of ATAC-Seq samples during GABAergic interneuron differentiation in Dravet Syndrome patient iPSCs.**

- **A.** Sequencing depth comparison from each sample.
- **B.** Pearson correlation matrix from technical duplicates of ATAC-Seq from all samples.
- **C.** Quantification of fraction of reads in peaks (FRiP) of ATAC-Seq in each condition. The dotted line indicates the cutoff was used.
- **D.** Transcription start site (TSS) enrichment score of ATAC-Seq in each sample.
- **E.** Genomic distribution of chromatin accessible regions for each sample.
- **F.** Principal component analysis of ATAC-Seq from each sample.
- **G.** Pearson correlation of gene expression from RNA-Seq and chromatin accessibility from ATAC-Seq.

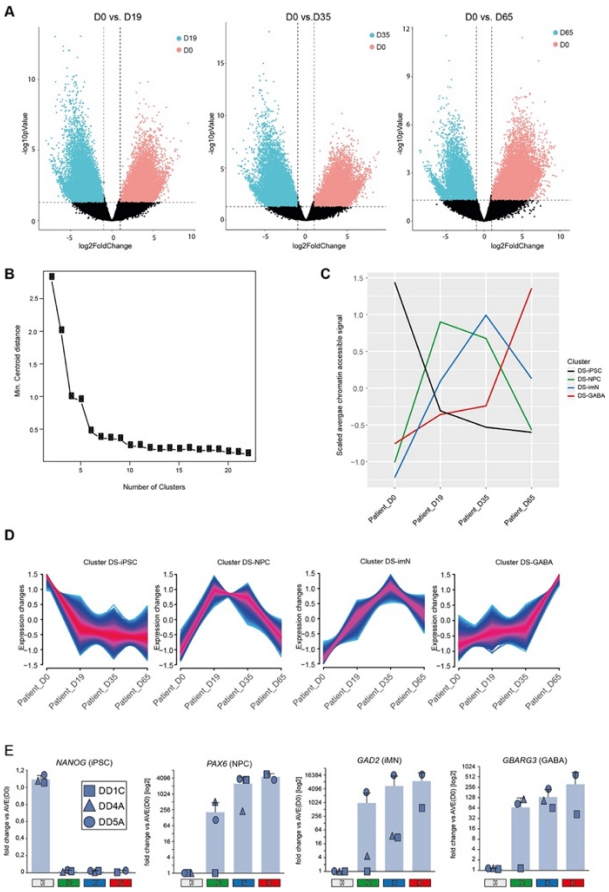


**Supplementary Figure 5: Chromatin accessibility cluster identification during GABAergic interneuron differentiation in Dravet Syndrome patient iPSCs.**

- **A.** Volcano plots show differential accessible chromatin peaks between D0 and different time points. D0 (n = 7798) vs. D19 (n = 5183); D0 (n = 10154) vs. D35 (n = 7239); D0 (n = 6909) vs. D65 (n = 5667). The dotted lines indicate the cutoff used to identify differential ATAC-Seq peaks.
- **B.** Variance with different numbers of clusters derived from chromatin accessibility during GABAergic interneuron differentiation in Dravet Syndrome patients.
- **C.** The scaled average chromatin accessibility during GABAergic interneuron differentiation from each cluster in Dravet Syndrome patients.
- **D.** The tendency of chromatin accessibility during GABAergic interneuron differentiation from each cluster in Dravet Syndrome patients.
- **E.** Expression of the four cluster markers *NANOG* (iPSC; D0), *PAX6* (PNC; D19), *GAD2* (imN; D35) and *BABRG3* (GABA; D65) quantified by qRT-PCR following GABAergic differentiation of control iPSC relative to expression of the housekeeping genes ACTB and GAPDH. Fold change data are presented as log2 [mean ΔΔCT(day Y)] ± SD and individual data points for each cell line are indicated (DS lines in blue: DD1C - square, DD4A - triangle, DD5A – circle please; see Methods for detail).

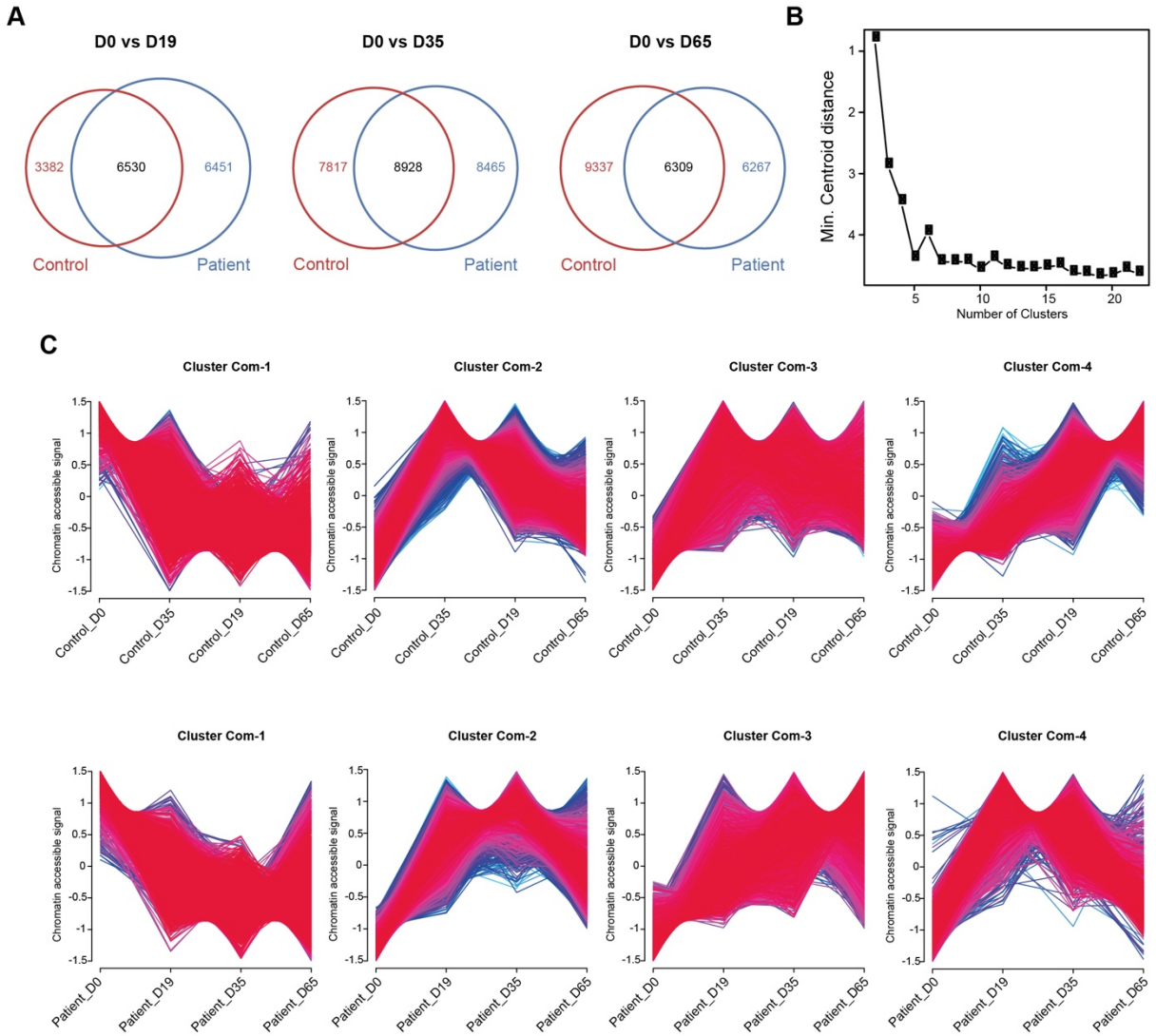


**Supplementary Figure 6: Identification of common chromatin accessibility between control and Dravet Syndrome patient iPSCs during GABAergic interneuron differentiation.**

- **A.** Venn diagrams showing the shared and distinct accessible chromatin peaks between control and patient samples.
- **B.** Variance with different numbers of clusters derived from common accessible chromatin regions between control and Dravet Syndrome patients.
- **C.** The tendency of chromatin accessibility from common accessible chromatin regions between control and Dravet Syndrome patients during GABAergic interneuron differentiation.

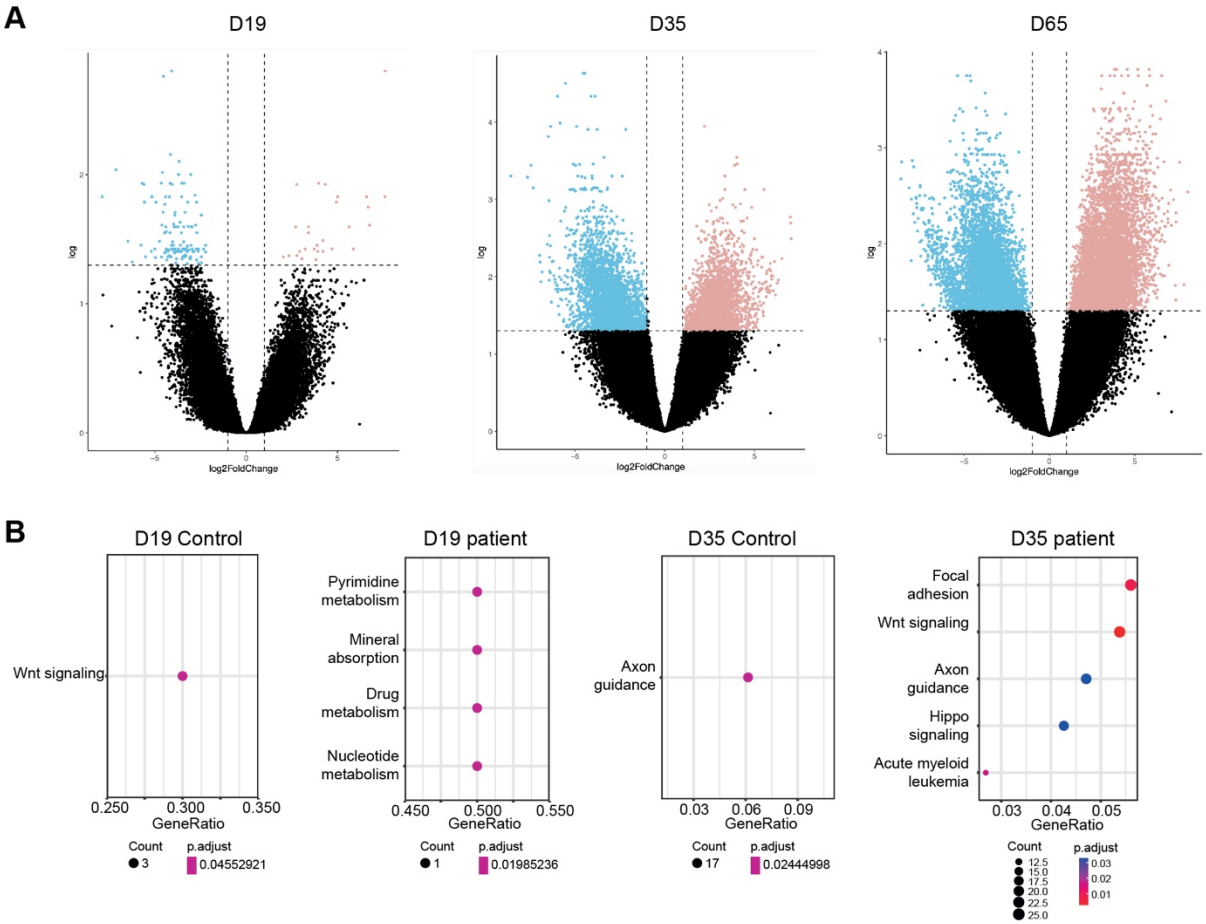


**Supplementary Figure 7: Identification of unique accessible chromatin region between control and Dravet Syndrome patient iPSCs during GABAergic interneuron differentiation.**

**A.** Volcano plot of differential accessible chromatin peaks between control and Dravet Syndrome (DS) patients at different stage of differentiation (NPC (Day 19), imN (Day 35) and GABAergic interneuron (Day 65)). Dotted lines indicate cutoff from fold change and false discovery rate.

**B.** KEGG signal pathway enrichments from unique accessible chromatin region in control and Dravet Syndrome patients at NPC (Day 19), imN (Day 35).

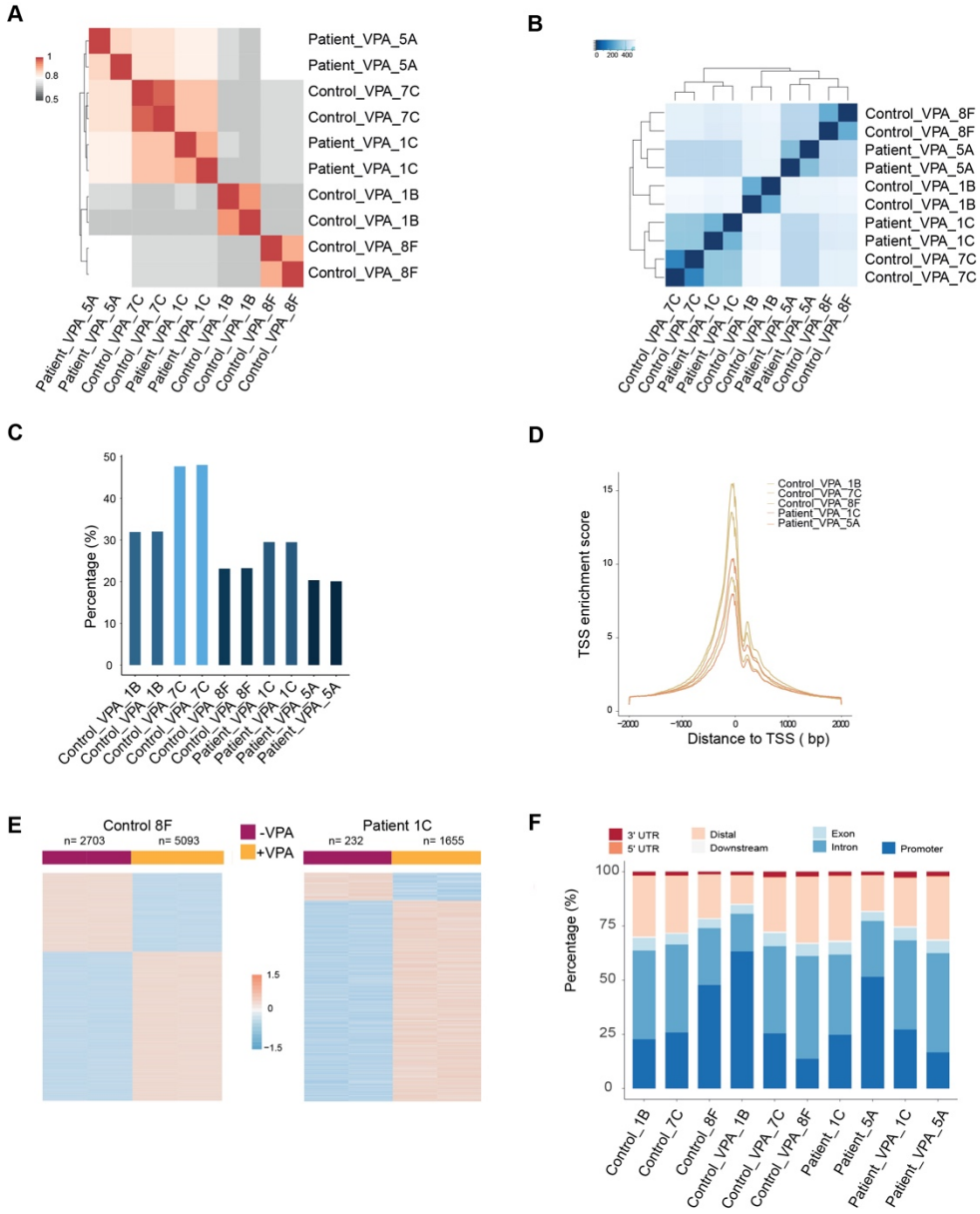


**Supplementary Figure 8: Valproic acid treatment reshapes chromatin accessibility of GABAergic interneurons.**

- **A.** Pearson correlation matrix from technical duplicates of ATAC-Seq of VPA treated control and Dravet Syndrome patient group.
- **B.** Distance matrix of ATAC-Seq from VPA treated control and Dravet Syndrome patient group.
- **C.** Quantification of fraction of reads in peaks (FRiP) of ATAC-Seq in each condition.
- **D.** Transcription start site (TSS) enrichment score of ATAC-Seq in each sample.
- **E.** Heatmap of differential chromatin accessible regions from VPA non-responsible group, consisting of one control sample and one Dravet Syndrome (DS) patient sample.
- **F.** Genomic distribution of chromatin accessible regions for each individual sample.

**Supplementary Table 1-7**:

**Supplementary Table 1: Identified differential ATAC-Seq peaks during GABAergic interneuron differentiation of Ctl-iPSC.**

**Supplementary Table 2: KEGG enrichment for each cluster during GABAergic interneuron differentiation of Ctl-iPSC.**

**Supplementary Table 3: Identified differential ATAC-Seq peaks during during GABAergic interneuron differentiation in Dravet Syndrome patient iPSCs.**

**Supplementary Table 4: KEGG enrichment for each cluster during GABAergic interneuron differentiation in Dravet Syndrome patient iPSCs.**

**Supplementary Table 5: Identified common ATAC-Seq peaks during GABAergic interneuron differentiation between control and Dravet Syndrome patient iPSCs.**

**Supplementary Table 6: Identified distinct ATAC-Seq peaks during GABAergic interneuron differentiation from control and Dravet Syndrome patient iPSCs.**

**Supplementary Table 7: Identified differential ATAC-Seq peaks between with and without VPA treatment.**